Universiteit
Leiden
The Netherlands

Development of new chemical tools to study the cannabinoid receptor type 2

Paus, L.V. de

Citation
Paus, L. V. de. (2024, May 22). *Development of new chemical tools to study the cannabinoid receptor type 2*. Retrieved from https://hdl.handle.net/1887/3754444

Version:	Publisher's Version
License:	Licence agreement concerning inclusion of doctoral thesis in the Institutional Repository of the University of Leiden
Downloaded from:	https://hdl.handle.net/1887/3754444

Note: To cite this publication please use the final published version (if applicable).

Chapter 2

Structural Basis of Selective Cannabinoid CB_2 Receptor Activation

Published as: Li X, Chang H, Bouma J, et al. Structural basis of selective cannabinoid CB2 receptor activation. Nat Commun. 2023;14(1):1447. doi:10.1038/s41467-023-37112-9

Structural Basis of Selective Cannabinoid CB_2 Receptor Activation

Introduction

Preparations of the plant *Cannabis sativa* have been used for centuries in the treatment of various diseases, including cancer and neuropathic pain.[1] The synthetic version of its psychoactive constituent, Δ^9-tetrahydrocannabinol (THC, Figure 2.1), is in FDA approved drugs Marinol® or Syndros® (dronabinol). The extracted version of THC is one of the active constituents of oromucosal spray Sativex® (nabiximols). These drugs are primarily used for the treatment of chemotherapy-induced nausea, enhancement of appetite in cachexic AIDS-patients, and to alleviate the spasticity and pain associated with multiple scleroses.[2–6] However, THC-based therapies are associated with clinically undesired psychotropic and cardiovascular adverse effects and challenging pharmacokinetic properties due to their high lipophilicity that may limit their therapeutic efficacy.[7–10]

THC exerts its therapeutic effects mostly via the G protein-coupled receptors (GPCRs) cannabinoid CB_1 and CB_2 receptors (CB_1R and CB_2R), which have 68% sequence identity in their seven transmembrane (TM) domains.[11] Both receptors are activated by the endogenous signaling lipids anandamide (AEA) and 2-arachidonoylglycerol (2-AG) (Figure 2.1), the two main endocannabinoids. The CB_1R, which is the most abundantly expressed GPCR in the central nervous system (CNS) is responsible for the psychotropic side effects of THC.[12–14] It plays a role in memory, learning, neurogenesis, neuronal migration, and synaptogenesis. Furthermore, its presence in many organ tissues belies more non-neurological functions.[15] The CB_2R is mainly found on the cells of the immune system and is upregulated under pathophysiological conditions.[16,17] Its activation in general is associated with anti-inflammatory responses in tissue injury of the liver, heart, kidney, colon, and brain as determined in various preclinical models.[18–22] Based on preclinical studies it is thought that selective CB_2R agonists may retain and exceed certain therapeutic properties of THC without inducing psychotropic side effects.[23]

Various academic and industrial groups have developed selective CB_2R ligands.[24] HU308 (Figure 2.1) was the first selective CB_2R agonist to be reported that displayed anti-inflammatory and analgesic properties in mouse models without inducing CNS-side effects.[18] However, poor physico-chemical properties (*e.g.* low solubility, high lipophilicity) of HU308, which has a calculated logarithm of octanol-water partition coefficient (cLogP) of 8.0[25], and its analogs prevented the successful clinical translation of this class of cannabinoid-based drugs.

A next generation of CB_2R ligands was developed with improved drug-like properties. For instance, Olorinab® (APD371, Figure 2.1) is the most polar CB_2R agonist reported to date with a cLogP of -0.4.[26] A phase 2a small-scale safety and tolerability trial in 14 patients with chronic abdominal pain associated with Crohn's disease showed mild-to-moderate adverse events and an improvement in abdominal pain scores.[27] Pyridinylbenzylimidazolidine-2,4-dione derivatives were previously disclosed as selective CB_2R agonists and their affinity studied, along with target binding kinetics and potency as a function of their lipophilicity, which resulted in the discovery of the orally available and peripherally restricted selective CB_2R agonist LEI-101 (Figure 2.1).[28–30] It is intriguing that the CB_2R binding pocket tolerates a wide array of ligands with very different scaffolds and hydrophobicity. For example, HU308 has a 2-billion-fold higher lipophilicity than APD371. Despite the tremendous progress in the field of CB_2R drug discovery, there is still a poor molecular understanding on how these CB_2R agonists selectively activate CB_2R over CB_1R.

Recently, three-dimensional structures of the CB_1R and CB_2R have been elucidated in both the active and inactive states by crystallography or cryo-electron microscopy (cryo-EM) and the binding modes of

diverse ligands and their activation mechanism were reported.[31–35] Remarkably, those structures revealed that CB_1R and CB_2R possess a highly similar, lipophilic orthosteric agonist binding pocket, which makes it challenging to explain the selective activation of CB_2R. To date, no structural studies with selective CB_2R agonists have been reported that could aid in understanding the molecular basis of CB_2R selectivity.

Here, LEI-102 is introduced as a novel, potent and selective CB_2R agonist with excellent physico-chemical and biological properties. LEI-102 was used in conjunction with CB_2R selective agonists APD371 and HU308, and non-selective agonist CP-55,940 to investigate the activation mechanism of CB_2R. This study combined ligand-target binding kinetics, site-directed mutagenesis, and cryo-EM methods. It was found that CB_2R has a distinct activation mechanism compared to CB_1R. Additionally, the physico-chemical properties of the ligands was found to influence their entry pathway into the receptor. Highly lipophilic ligands, such as HU308 and the endocannabinoids, may reach the binding pocket through the membrane, whereas more polar ligands, such as LEI-102, APD371 and CP-55,940, enter the receptor via an alternative route. Furthermore, it was shown that the favorable physico-chemical properties of LEI-102 and CB_2R selectivity underscore its promising *in vivo* efficacy via oral administration in a chemotherapy-induced nephropathy model without inducing CNS-mediated side effects. Together, these studies enhance the current insights of how certain physico-chemical properties of ligands translate to *in vivo* activity and changes their engagement to GPCRs.

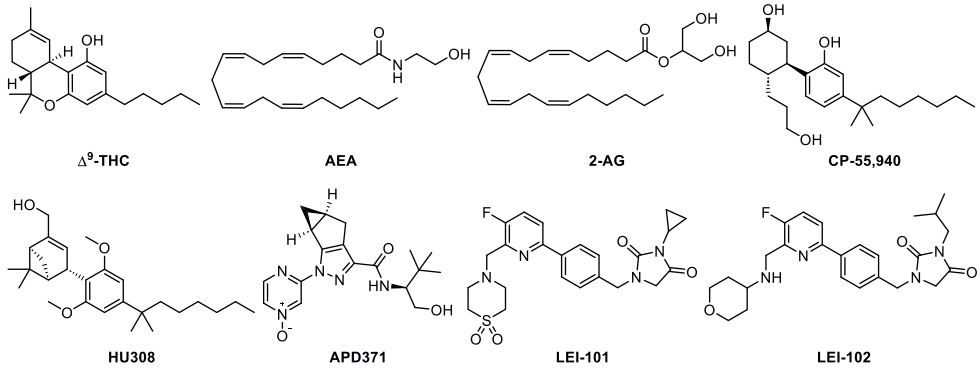

Figure 2.1 The chemical structures of the main constituent of Cannabis sativa Δ^9-tetrahydrocannabinol (THC), and the two major endocannabinoids anandamide (AEA) and 2-arachidonoylglycerol (2-AG), as well as of non-selective CBR agonist CP-55,940 and CB_2R agonists HU308, APD371, LEI-101 and LEI-102.

Results

LEI-102 as a high affinity and potent CB_2R--selective agonist

To obtain a novel CB_2R agonist with beneficial physico-chemical properties, LEI-102, a pyridinylbenzylimidazolidine-2,4-dione derivative, was designed and synthesized (Scheme 2.1). LEI-102 combined an isobutyl substituent on the imidazolidine with an aminotetrahydropyran to replace the cyclopropyl and thiomorpholine 1,1-dioxide in LEI-101, respectively.[30]

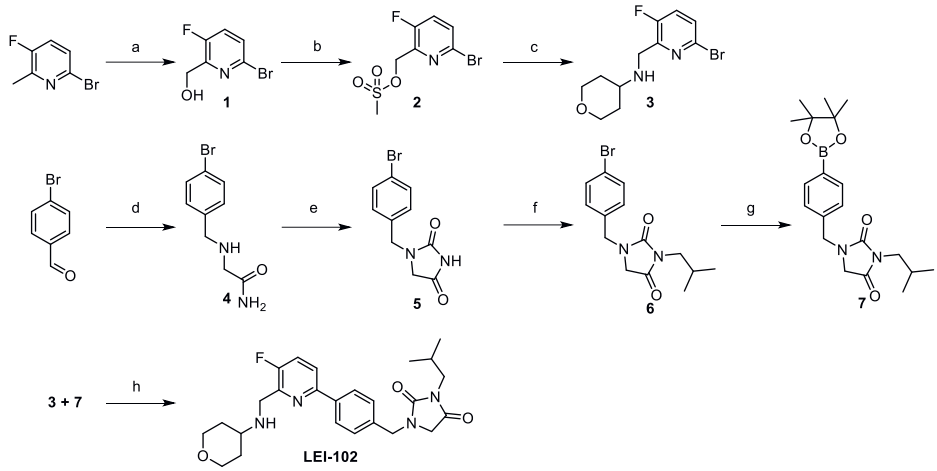

Scheme 2.1 Synthetic route of LEI-102. Reagents and conditions: a) Step 1: *m*-CPBA (1.8 eq), 0 °C-RT, DCM, 4 days; Step 2: TFAA (2.2 eq), 55 °C, 3 h; Step 3: K_2CO_3 (2.4 eq), THF:MeOH (20:1), 17 h, 35% (three steps); b) Et_3N (2.3 eq), MsCl (1.7 eq), THF, 0 °C-RT, 1 h, 75%; c) K_2CO_3 (2.2 eq), tetrahydro-2H-pyran-4-amine (1.3 eq), ACN, 50 °C, 3 h, 67%; d) Step 1: 2-aminoacetamide hydrochloride (1.0 eq), NaOH (1.1 eq), MeOH:H_2O (5:1), RT, 18 h; Step 2: $NaBH_4$ (2.1 eq), 18 h, 91% (two steps); e) CDI (2.1 eq), DMAP (2.1 eq), ACN, 60 °C, 70 h, 37%; f) K_2CO_3 (3.0 eq), 1-bromo-2-methylpropane (2.0 eq), DMF, RT, 20 h, 88%; g) KOAc (4.4 eq), bis(pinacolato)diboron (1.5 eq), Pd(dppf)Cl_2 (0.06 eq), DMF, 75 °C, 20 h; h) **3** (1.0 eq), **7** (1.5 eq), K_2CO_3 (6.0 eq), $Pd(PPh_3)_4$ (0.1 eq), toluene:EtOH (4:1), 75 °C, 18 h, 45% (two steps).

LEI-102 has a cLogP of 2.1 as calculated by ChemDraw 19.0 (Table 2.1). The inhibitory constant (pK_i), potency (pEC_{50}) and intrinsic activity (E_{max}) of LEI-102 were determined in [^{3}H]-RO6957022 displacement assays on stably expressing CB_2R membranes and [^{35}S]GTPγS G protein activation assays using HEK293T membranes transiently expressing recombinant hCB_2R or hCB_1R, respectively (Table 2.2). APD371, HU308, CP-55,940 and the endocannabinoids AEA and 2-AG were also explored. LEI-102 had a high binding affinity for CB_2R (pKi = 8.0 ± 0.1) and was more potent than the selective CB_2R agonists APD371 and HU308. LEI-102 did not bind CB_1R, thereby showing at least 1000-fold selectivity (Table 2.5). In G protein activation assays, LEI-102 activated the receptor as a partial agonist (E_{max} 76 ± 1 %) with a pEC_{50} value of 6.9 ± 0.2 (Table 2.2).

Table 2.1 Physico-chemical properties of the investigated ligands.

Compound	CLogP	SLogP	TPSA (Å)	MW (g/mol)	Num RotatableBonds	NumHBD	NumHBA
Δ^9-THC	7.24	5.74	29.5	314.5	4	1	2
2-AG	6.89	5.03	66.8	378.6	17	2	4
AEA	6.18	5.24	49.3	347.5	16	2	2
CP-55,940	5.82	5.66	60.7	376.6	10	3	3
HU308	8.00	6.63	38.7	414.6	10	1	3
APD371	-0.35	0.70	107.0	357.4	4	2	6
LEI-102	2.07	3.58	74.8	454.5	8	1	5
LEI-101[30]	0.89	-	90.4	472.5	6	0	6

All values calculated using RDKit KNIME nodes version 4.5.0.v202207051536, apart from CLogP which was calculated using ChemDraw 19.0. For LEI-101 all values were calculated with Chemdraw 22.2.0.

Table 2.2 Functional Activity, Affinity and Kinetic Parameters of Synthetic Agonists and Endocannabinoids on hCB_2R.

Compound	pEC_{50}[a]	E_{max} (%)[b]	pK_i (K_i, nM)[c]	k_{on} ($M^{-1}s^{-1}$)[d]	ET (s)[e]	k_{off} (s^{-1})[f]	RTD (min)[g]	K_D (nM)[h]
LEI-101[30,i]	6.6 ± 0.2	65 ± 8	6.51 ± 0.1 (309.0)	$(3.0 \pm 1.1) \times 10^4$	33.3 ± 8.91	$(2.1 \pm 0.5) \times 10^{-3}$	8.8 ± 1.6	76 ± 10
LEI-102	6.9 ± 0.2	76 ± 1	8.0 ± 0.1 (9.7)	$(6.3 \pm 1.1) \times 10^4$	16.0 ± 2.82	$(1.0 \pm 0.2) \times 10^{-3}$	16 ± 3.3	16.5
APD371	7.9 ± 0.1	134 ± 12	7.5 ± 0.1 (35.3)	$(2.5 \pm 0.4) \times 10^4$	40.1 ± 5.90	$(3.7 \pm 0.5) \times 10^{-4}$	45 ± 6.6	14.9
HU308	7.1 ± 0.2	91 ± 8	7.0 ± 0.1 (92.4)	$(7.0 \pm 2.3) \times 10^3$	143 ± 47.9	$(2.3 \pm 0.4) \times 10^{-4}$	71 ± 11	33.7
CP-55,940	8.5 ± 0.3	98 ± 4	8.9 ± 0.1 (1.4)	$(1.8 \pm 0.4) \times 10^6$	0.57 ± 0.13	$(5.2 \pm 0.9) \times 10^{-4}$	32 ± 5.5	0.3
AEA	6.3 ± 0.2	60 ± 5	6.3 ± 0.1 (484.5)	$(6.6 \pm 0.5) \times 10^3$	152 ± 10.4	$(2.4 \pm 0.1) \times 10^{-3}$	6.8 ± 0.4	371.7
2-AG	5.9 ± 0.1	93 ± 22	7.0 ± 0.1 (97.3)	$(5.3 \pm 1.0) \times 10^4$	18.8 ± 3.61	$(2.3 \pm 0.3) \times 10^{-3}$	7.4 ± 1.0	42.7

[a, b] Potency (pEC_{50}) and efficacy (E_{max}) values were obtained from [^{35}S]GTPγS assays on HEK293T membranes transiently expressing CB_2R WT. The percentage maximum effect (E_{max} in %) was calculated compared to CP-55,940. [c, d, f] Binding affinities (pK_i), association (k_{on}) and dissociation (k_{off}) rate constants were determined in [^{3}H]-RO6957022 binding assays on CHOK1_hCB_2R_bgal membranes at 10 °C. [e] Engagement time (ET) of the compound to the receptor at 1 μM agonist was determined by $ET = 1/(k_{on} \cdot 1 \times 10^{-6})$ and is expressed in seconds (s), whereas k_{on} is expressed in $M^{-1}s^{-1}$. [g] Residence time (RTD) was determined by $RTD = 1/(60 \cdot k_{off})$ and is expressed in min, whereas k_{off} is expressed in s^{-1}. [h] Kinetic K_D values, defined by $K_D = k_{off}/k_{on}$. Values represent the mean ± SEM of at least three independent experiments performed in duplicate. [i]LEI-101 data was obtained from literature and values were measured on CHO_K1_hCB_2R_bgal membranes.

Distinct target binding kinetic profiles of CB_2R agonists

For the quantification of the ligand-target binding kinetic parameters of the agonists, displacement and competition association assays with [^{3}H]-RO6957022 were performed on CHO membranes stably over-expressing hCB_2R_bgal (Table 2.1). The equilibrium K_i and kinetic K_D values were well correlated, validating the competition association assay. The determined dissociation rate constants (k_{off}) of all agonists was converted into Residence Time Distribution (RTD). LEI-102 had an RTD of 16 min, which was around half that of APD371 (45 min) and CP-55,940 (32 min), whereas HU308 had the longest RTD at the receptor of 71 min (Table 2.1). Endocannabinoids 2-AG and AEA had the shortest RTD, both approximately 7 min. The association rate constants (k_{on}) varied greatly between the different agonists, ranking from fast to slow engagement CP-55,940 > LEI-102 > 2-AG > APD371 > HU308 = AEA. The calculated engagement time (ET) to CB_2 at 1 µM of each agonist further emphasized that CP-55,940 arrived at CB_2R within one second, whereas APD371, LEI-102 and 2-AG needed between 16 and 40 s to reach the CB_2R binding site. Interestingly, HU308 and AEA took 143 and 152 s to bind CB_2R, respectively. Due to the distinct target-binding kinetic profiles found for the four synthetic CB_2R agonists the choice was made to elucidate their binding poses in CB_2R with cryo-EM.

Overall similar structural comparison of CB_2R-G_i in complex with different agonists

To obtain the stable complex sample of CB_2R-G_i bound with LEI-102, APD371, HU308, or CP-55,940, a similar procedure was used as for the complex preparation previously described for AM12033-CB_2R-G_i (PDB: 6KPF). Single particle analysis of the cryo-EM samples yielded a normal global map for CB_2R-LEI-102-G_i-scFv16, CB_2R-APD371-G_i-scFv16, CB_2R-HU308-G_i-scFv16 and CB_2R-CP-55,940-G_i-scFv16, complex, at 2.9 Å, 3.0 Å, 3.0 Å and 2.9 Å, respectively (Figure 2.2). The ligand, receptor and G protein in the isolated complex were clearly visible in the cryo-EM maps (Figure 2.2). The overall structures of the four complexes were comparable, with root mean square deviation (RMSD) of the Cα atoms of the receptors are around 0.35 Å. The ligand binding interfaces of the four CB_2R and G_i complexes were similar to each other, and to those of the previous AM12033-CB_2R-G_i or WIN55212-2-CB_2R-G_i complex structures.

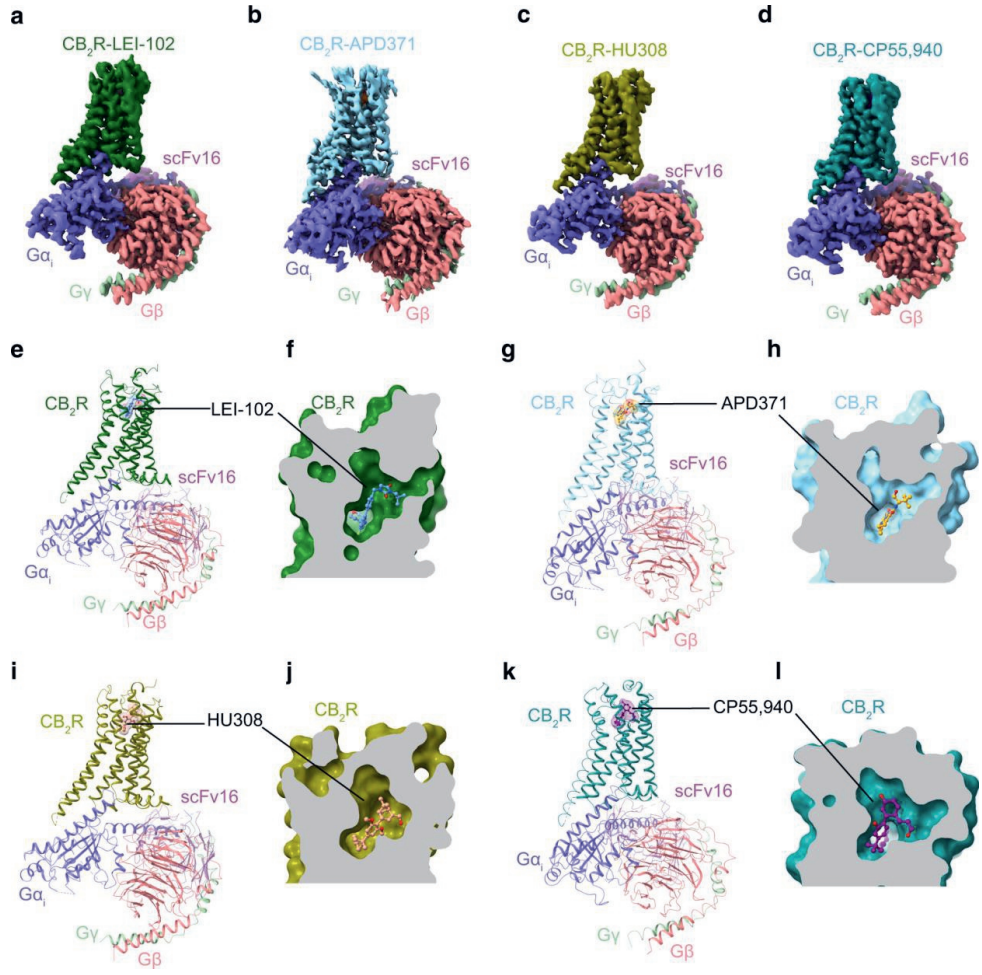

Figure 2.2 Cryo-EM structures of CB_2R-G_i complexes (A-D) Cryo-EM density maps of (A) LEI-102 (Dark green), (B) APD371 (Sky blue), (C) HU308 (Olive) and (D) CP-55,940 (Teal) bound CB_2R in complex with $G_{\alpha i}$ (Slate), Gβ (Salmon), Gγ (Pale green), scFv16 (Violet purple). (E-L) Overall structures of CB_2R-G_i complexes and enlarged view of orthosteric pocket of (F) LEI-102, (H) APD371, (J) HU308 and (L) CP-55,940 using the same color codes as (A-D), with agonists shown as Cornflower blue (LEI-102), Orange (APD371), Dark salmon (HU308) and Purple (CP-55,940) sticks, respectively.

The binding mode of LEI-102 in CB_2R

A clear electron density in the orthosteric ligand binding pocket in the LEI-102-CB_2R-G_i complex resulted in the unambiguously defined binding pose of LEI-102. LEI-102 predominantly interacted with the residues in the binding pocket via hydrophobic interactions (Figure 2.3A). The isobutyl substituent of LEI-102 showed interactions with residues $S90^{2.60}$ (Ballesteros-Weinstein numbering in superscript), $F106^{3.25}$, $K109^{3.28}$, and $I110^{3.29}$ in CB_2R. The imidazolidine-2,4-dione forms π-π interaction with $F94^{2.64}$ and showed further hydrophobic interactions with $F106^{3.25}$ and $P184^{ECL2}$. The benzyl formed an aromatic interaction with $F183^{ECL2}$, and hydrophobic interactions with $F87^{2.57}$ and $S285^{7.39}$. The phenyl ring in the core of LEI-102 formed a cation π interaction with $F183^{ECL2}$ and T-shaped π-π interaction with $F281^{7.35}$. The pyridine had hydrophobic contacts with $F117^{3.36}$ and $W258^{6.48}$. The aminotetrahydropyran sidechain protruded into the long channel and formed hydrophobic interactions with residues $I110^{3.29}$,

$T114^{3.33}$, $I186^{ECL2}$, $Y190^{5.39}$, $L191^{5.40}$, $W194^{5.43}$ and $M265^{6.55}$. Additionally, a hydrogen bond was formed with $T114^{3.33}$ (Figure 2.3A).

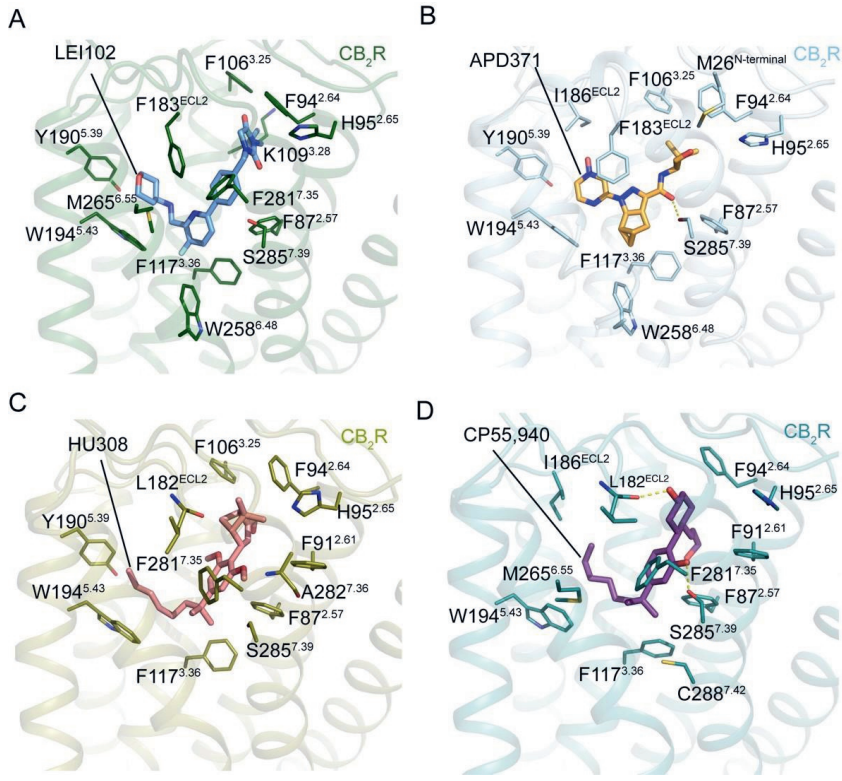

Figure 2.3 Key interactions between CB_2R structure and agonists (A-D) Key residues involved in (A) LEI-102 (cornflower blue) with CB_2R-G_i (dark green), (B) APD371 (orange) with CB_2R-G_i (sky blue), (C) HU308 (dark salmon) with CB_2R-G_i (olive) and (D) CP-55,940 (purple) with CB_2R-G_i (teal) binding in the complex structures. The amino acids involved interactions are showing sticks, hydrogen bonds are highlighted with yellow dashed lines.

The binding mode of APD371 in CB_2R

APD371 mainly formed hydrophobic and aromatic interactions with residues from ECL2, TM2, TM3, TM5, TM6 and TM7 (Figure 2.3B). The carbonyl group of APD371 formed a putative hydrogen bond with $S285^{7.39}$ and a hydrophobic interaction with $F87^{2.57}$. The pyrazole and pyrazine cores of APD371 formed aromatic interaction with $F183^{ECL2}$. Furthermore, the pyrazine core formed hydrophobic contacts with $T114^{3.33}$, $I186^{ECL2}$, $L191^{5.40}$ and $W194^{5.43}$. The (*S*)-1-hydroxy-3,3-dimethylbutyl head formed hydrophobic contacts with residues $M26^{N\text{-terminus}}$, $S90^{2.60}$, $F94^{2.64}$, $F106^{3.25}$, $I110^{3.29}$ and $V113^{3.32}$. The cyclopropyl group formed hydrophobic contacts with $F117^{3.36}$, $W194^{5.43}$, $W258^{6.48}$ and $V261^{6.51}$.

The binding mode of HU308 in CB_2R

The interactions between HU308 and CB_2R were hydrophobic, including residues from ECL2, TM2, TM3, TM5, TM6 and TM7 (Figure 2.3C). The phenyl of 2,6-dimethoxyphenyl core formed hydrophobic interactions with $F87^{2.57}$, $F183^{ECL2}$ and $S285^{7.39}$, the C2-methoxy formed hydrophobic contacts with $A282^{7.36}$ and $S285^{7.39}$, and the C6-methoxy formed hydrophobic contacts with $I110^{3.29}$, $V113^{3.32}$ and $T114^{3.33}$, respectively. The dimethylheptyl chain of HU308 extended into the long channel and formed hydrophobic interactions with residues from ECL2 ($F183^{ECL2}$), TM3 ($T114^{3.33}$, $F117^{3.36}$), TM5 ($W194^{5.43}$). The 1,1-dimethyl formed hydrophobic interactions with residues $F87^{2.57}$, $F117^{3.36}$, $F281^{7.35}$ and $S285^{7.39}$.

The bicyclic head of HU308 formed hydrophobic interactions with M26$^{N\text{-terminus}}$, F106$^{3.25}$, I110$^{3.29}$, S90$^{2.60}$, F94$^{2.64}$, P184^{ECL2} and the 2-methanol formed a hydrophobic interaction with F94$^{2.64}$.

The binding mode of CP-55,940 in CB_2R

CP-55,940 adopted an L-shape conformation in the orthosteric binding pocket (Figure 2.3D). The cyclohexanol group formed hydrophobic interactions with F94$^{2.64}$, L182^{ECL2}, F183^{ECL2}, and P184^{ECL2}. The hydroxyl group established a hydrogen bond with L182^{ECL2} and the hydroxypropyl formed hydrophobic contacts with F87$^{2.57}$, S90$^{2.60}$, F91$^{2.61}$, I110$^{3.29}$, and V113$^{3.32}$. The phenol core formed hydrophobic interactions with F87$^{2.57}$, F183^{ECL2}, F281$^{7.35}$ and S285$^{7.39}$, and its hydroxyl additionally formed a hydrogen bond with S285$^{7.39}$. The dimethyl formed hydrophobic interactions with F183^{ECL2}, F281$^{7.35}$, M265$^{6.55}$, F87$^{2.57}$, F117$^{3.36}$ and C288$^{7.42}$. The dimethylheptyl alkyl chain of CP-55,940 extended into the long channel and formed hydrophobic interactions with residues I110$^{3.29}$, F183^{ECL2}, I186^{ECL2}, W194$^{5.43}$, T114$^{3.33}$ and F117$^{3.36}$.

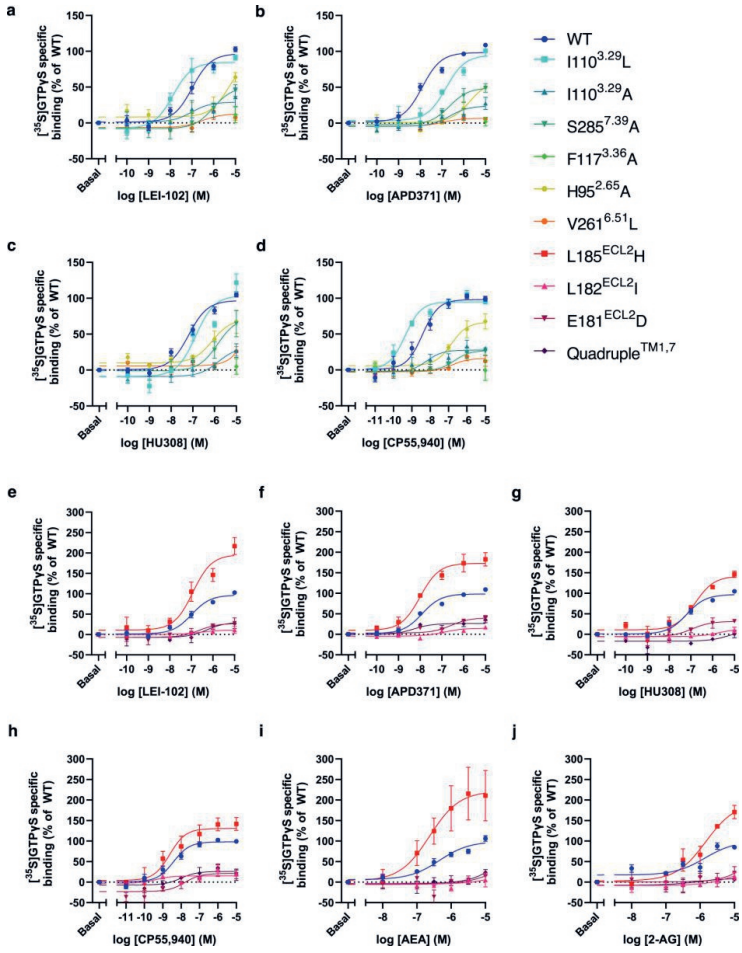

Figure 2.4 Characterization of G Protein activation of wild type (WT) and mutant CB_2R by synthetic agonists and endocannabinoids. (A-D) Dose-response curves for G protein activation of WT and mutants that are located in the CB_2R binding pocket by (A) LEI-102, (B) APD371, (C) HU308 and (D) CP-55,940. (E-J) Dose response curves for G protein activation of WT and mutants that are proposed to be involved in ligand entry of CB_2R via either the ECL2 or membrane access by (E) LEI-102, (F) APD371, (G) HU308, (H) CP-55,940, (I) AEA and (J) 2-AG. (A-J) The maximum activation level of WT CB_2R was set

to 100% while the basal levels were set to 0%. Data are presented as mean ± SEM of at least three individual experiments performed in duplicate.

LEI-102 and APD371 require $H95^{2.65}$ for G protein activation in CB_2R

To study the mechanism of CB_2R activation, five residues in the binding pocket were further characterized based on the complex structures (Figure 2.3). Six CB_2R mutants were created, *i.e.* four residues ($S285^{7.39}$, $H95^{2.65}$, $I110^{3.29}$ and $F117^{3.36}$) were replaced by alanine, as these are conserved between CB_2R and CB_1R, and two others ($I110^{3.29}$, $V261^{6.51}$) were substituted by the CB_1R reciprocal residue leucine. All mutants were sufficiently expressed at the cell surface as determined with an ELISA (Figure 2.5, Table 2.3). To characterize the binding mechanisms of LEI-102, APD371, HU308 and CP-55,940, their responses were investigated by [^{3}H]CP-55,940 displacement and [^{35}S]GTPγS binding assays. Of note, in the [^{3}H]CP-55,940 displacement assay, only the CB_2R-$I110^{3.29}$L mutant showed a sufficient binding window (data not shown). This prevented the affinity determination of the four agonists on other mutant receptors. Five mutant receptors, except CB_2R-$F117^{3.36}$A, were still active in the [^{35}S]GTPγS functional assay for study of the receptor activation mechanism (Figure 2.4A-D, Table 2.4). All four synthetic agonists were unable to activate CB_2R-$F117^{3.36}$A, which indicated an important role of this residue in the activation of CB_2R.

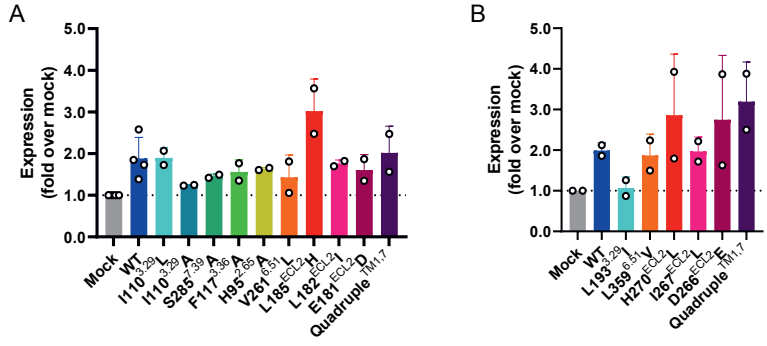

Figure 2.5 Cell Surface Receptor Expression. Receptor expression as determined by ELISA for (A) CB_2R and (B) CB_1R wild type (WT) and mutants. Data are expressed as mean ± SD of at least two experiments performed in quintuplicate.

Table 2.3 Cell surface expression levels of cannabinoid receptor constructs in ELISA.

	CB_2R	Expression (fold over Mock)	CB_1R	Expression (fold over Mock)
	WT	1.9 ± 0.5	WT	2.0 ± 0.2
Binding pocket	$I110^{3.29}L$	1.9 ± 0.2	$L193^{3.29}I$	1.1 ± 0.3
	$I110^{3.29}A$	1.2 ± 0.0	$L193^{3.29}A$	n.d.
	$S285^{7.39}A$	1.5 ± 0.1	$S383^{7.39}A$	n.d.
	$F117^{3.36}A$	1.6 ± 0.3	$F200^{3.36}A$	n.d.
	$H95^{2.65}A$	1.6 ± 0.0	$H178^{2.65}A$	n.d.
	$V261^{6.51}L$	1.4 ± 0.5	$L359^{6.51}V$	1.9 ± 0.5
Ligand entry	$L185^{ECL2}H$	3.0 ± 0.8	$H270^{ECL2}L$	2.9 ± 1.5
	$L182^{ECL2}I$	1.8 ± 0.1	$I267^{ECL2}L$	2.0 ± 0.4
	$E181^{ECL2}D$	1.6 ± 0.4	$D266^{ECL2}E$	2.7 ± 1.6
	$Quadruple^{TM1,7}$	2.0 ± 0.6	$Quadruple^{TM1,7}$	3.2 ± 1.0

Mutations are shown in the numbering of the cannabinoid CB2 (CB2R) or CB1 receptor (CB1R) amino acid sequence as well as the Ballesteros and Weinstein GPCR numbering system. Data are presented as fold over mock (empty pcDNA3.1 vector) and are mean ± SD of at least two individual experiments performed in quintuplicate. n.d. is not determined.

Table 2.4 The Affinity and Potency of the Agonists on the CB_2R mutants.

CB_2R	LEI-102		CP-55,940		HU308		APD371	
Construct	**pK_i**	**pEC_{50}**	**pK_i**	**pEC_{50}**	**pK_i**	**pEC_{50}**	**pK_i**	**pEC_{50}**
WT	7.5 ± 0.1	6.9 ± 0.2	9.2 ± 0.2	8.5 ± 0.3	7.8 ± 0.2	7.1 ± 0.2	8.0 ± 0.0	7.9 ± 0.1
$I110^{3.29}L$	7.9 ± 0.0	7.8 ± 0.1**	9.1 ± 0.1	9.4 ± 0.2	7.3 ± 0.1	6.7 ± 0.4	7.1 ± 0.0***	6.7 ± 0.3
$I110^{3.29}A$	n.d.	7.0 ± 0.6	n.d.	8.7 ± 0.4	n.d.	6.4 ± 0.5	n.d.	6.6 ± 0.6
$S285^{7.39}A$	n.d.	6.3 ± 0.3	n.d.	6.7 ± 0.1**	n.d.	5.9 ± 0.1***	n.d.	6.5 ± 0.3
$F117^{3.36}A$	n.d.	n.d.	n.d.	n.d.	n.d.	n.d.	n.d.	n.d.
$H95^{2.65}A$	n.d.	<5	n.d.	6.9 ± 0.2**	n.d.	6.6 ± 0.6	n.d.	5.7 ± 0.2**
$V261^{6.51}L$	n.d.	6.4 ± 0.0	n.d.	<5	n.d.	<5	n.d.	6.9 ± 0.2*
$L185^{ECL2}H$	7.3 ± 0.1	6.9 ± 0.1	9.4 ± 0.1	8.9 ± 0.4	7.2 ± 0.0	6.8 ± 0.2	7.7 ± 0.1	8.0 ± 0.1
$L182^{ECL2}I$	n.d.	7.4 ± 0.8	n.d.	8.8 ± 0.8	n.d.	<5	n.d.	6.6 ± 0.4
$E181^{ECL2}D$	n.d.	6.9 ± 0.6	n.d.	7.9 ± 0.5	n.d.	7.0 ± 0.7	n.d.	6.9 ± 0.6
$Quadruple^{TM1,7}$	6.8 ± 0.2	6.2 ± 0.2	9.2 ± 0.1	8.1 ± 0.2	7.1 ± 0.4	n.d.	6.7 ± 0.3	8.4 ± 0.1

Mutants that gave no dpm window could not have their potency determined (n.d. not determined). Mutations are shown in the numbering of the cannabinoid receptor 2 amino acid sequence as well as the Ballesteros and Weinstein GPCR numbering system. pEC_{50} <5 was reported when the curve fit was not finished. Values are presented as the mean ± SEM of at least three independent experiments performed in duplicate. One-way Welch ANOVA with Dunnett's T3 posthoc test or Welch's t-test was used to analyze differences in pEC_{50} and E_{max} values compared to WT (*p < 0.05, ** p < 0.01, *** p < 0.001).

Table 2.5 The Affinity and Potency of the Agonists on the CB_1R mutants.

CB_1R	LEI-102		CP-55,940		HU308		APD371	
Construct	**Displacement (%)**	**Potency (fold over basal)**	**pK_i**	**Potency (fold over basal)**	**Displacement (%)**	**Potency (fold over basal)**	**Displacement (%)**	**Potency (fold over basal)**
WT	6 ± 7	1.0 ± 0.1	8.2 ± 0.0	1.2 ± 0.1	17 ± 7	0.8 ± 0.0	-19 ± 17	1.0 ± 0.0
$L359^{6.51}V$	41 ± 10	1.1 ± 0.1	8.3 ± 0.1	1.4 ± 0.2	25 ± 6	0.9 ± 0.1	18 ± 9	1.1 ± 0.1
$H270^{ECL2}L$	46 ± 3	1.2 ± 0.0	8.3 ± 0.1	1.6 ± 0.1	47 ± 5	1.2 ± 0.1*	8 ± 3	1.1 ± 0.0
$I267^{ECL2}L$	-7 ± 19	1.0 ± 0.0	8.4 ± 0.1	1.0 ± 0.0	25 ± 3	0.8 ± 0.0	-24 ± 17	0.9 ± 0.0
$D266^{ECL2}E$	34 ± 5	1.1 ± 0.1	8.4 ± 0.1	1.4 ± 0.1	38 ± 10	0.8 ± 0.1	12 ± 7	0.9 ± 0.1
$Quadruple^{TM1,7}$	-13 ± 22	1.2 ± 0.1	8.0 ± 0.2	1.8 ± 0.1*	26 ± 10	0.9 ± 0.0	0 ± 25	1.1 ± 0.0

Affinity is expressed as pK_i for CP-55,940, but as displacement (receptor occupancy by agonist at 10 μM) for the CB_2R-selective agonists. The Potency is displayed as fold over basal (with basal the endogenous activity of the mutant). Mutations are shown in the numbering of the cannabinoid receptor 2 amino acid sequence as well as the Ballesteros and Weinstein GPCR numbering system. pEC_{50} <5 was reported when the curve fit was not finished. Values are presented as the mean ± SEM of at least three independent experiments performed in duplicate. One-way Welch ANOVA with Dunnett's T3 posthoc test or Welch's t-test was used to analyze differences in pEC_{50} and E_{max} values compared to WT (*p < 0.05, ** p < 0.01).

The potency of LEI-102 was significantly increased at the CB_2R-$I110^{3.29}L$ mutant to a pEC_{50} value of 7.8 ± 0.1 in the G protein activation assay, while the binding affinity remained similar to wild type (WT) receptor (Figure 2.4A, Table 2.4). Three mutations CB_2R-$I110^{3.29}A$, CB_2R-$S285^{7.39}A$ and CB_2R-$V261^{6.51}L$ had no significant effect on the potency of LEI-102 in the functional assay. In contrast, the potency on mutant receptor CB_2R-$H95^{2.65}A$ was significantly reduced for LEI-102. No gain in binding affinity for the swap mutant in CB_1R-$L359^{6.51}V$ was found with LEI-102 (Table 2.5).

APD371 acted as a full CB_2R agonist with a pEC_{50} value of 7.9 ± 0.1 and a higher maximal activation compared to that of CP-55,940 in the functional assay (Table 2.2). Mutant receptor CB_2R-$I110^{3.29}L$ did not affect the G protein response of APD371 (Figure 2.4B, Table 2.4), while the binding affinity was significantly reduced to a pK_i of 7.1 ± 0.0 (Table 2.4). APD371 potency was not affected by mutant receptors CB_2R-$I110^{3.29}A$ or CB_2R-$S285^{7.39}A$. The responses of APD371 for CB_2R-$H95^{2.65}A$ and CB_2R-$V261^{6.51}L$ were significantly impacted with 158-fold and 10-fold drop in potency, respectively (Table 2.4).

It is apparent that CB_2R-$H95^{2.65}$ has a crucial role in G protein activation of CB_2R by LEI-102 and APD371. Additionally, LEI-102 activation was increased for the CB_2R-$I110^{3.29}L$ mutant, while APD371 activation relied on CB_2R-$V261^{6.51}$.

An important role for $S285^{7.39}$ and $V261^{6.51}$ in CB_2R activation by HU308 and CP-55,940

The potency and affinity of HU308 on CB_2R were not affected by the CB_2R-$I110^{3.29}L$ swap mutant (Figure 2.4C, Table 2.4). In addition, activation of mutant receptors CB_2R-$I110^{3.29}A$ and CB_2R-$H95^{2.65}A$ by HU308 was not affected with pEC_{50} values of 6.4 ± 0.5 and 6.6 ± 0.6, respectively. The maximum activation level of mutant receptor CB_2R-$S285^{7.39}A$ was unaffected compared to WT receptor, but a significant 15-fold loss in potency was observed. Lastly, CB_2R-$V261^{6.51}L$ had a significant loss of potency, *i.e.* more than 120-fold lower (Figure 2.4C, Table 2.4).

Similar to HU308, the potency of CP-55,940 on CB_2R was not affected by the CB_2R-$I110^{3.29}$ mutations compared to WT in the G protein activation assay, nor was its binding affinity for CB_2R-$I110^{3.29}L$ (Figure 2.4D, Table 2.4). In response to CP-55,940, mutant receptors CB_2R-$S285^{7.39}A$ and CB_2R-$V261^{6.51}L$ were significantly affected with decreased pEC_{50} values of 6.7 ± 0.1 and <5, respectively. Moreover, the potency of CP-55,940 was significantly affected on the CB_2R-$H95^{2.65}A$ with a 40-fold decrease compared to WT receptor (Figure 2.4D, Table 2.4). No gain in potency or affinity was observed for the swap mutant CB_1R-$L359^{6.51}V$ for either HU308 or CP-55,940 (Table 2.5).

Taken together, this showed that CB_2R-$S285^{7.39}$ and CB_2R-$V261^{6.51}$ were crucial for HU308 and CP-55,940 to activate the G protein at CB_2R, where CP-55,940 additionally required an interaction with CB_2R-$H95^{2.65}$.

Table 2.6 The Affinity and Potency of the Endocannabinoids on both CB_2R and CB_1R.

		AEA		2-AG	
CB_2R	**Construct**	**pK_i**	**pEC_{50}**	**pK_i**	**pEC_{50}**
	WT	6.2 ± 0.1	6.3 ± 0.2	5.8 ± 0.1	5.9 ± 0.1
	$L185^{ECL2}H$	6.3 ± 0.1	6.6 ± 0.0	6.4 ± 0.2	5.9 ± 0.2
	$L182^{ECL2}I$	n.d.	<5	n.d.	<5
	$E181^{ECL2}D$	n.d.	<5	n.d.	<5
	$Quadruple^{TM1,7}$	5.6 ± 0.3	<5	<5	<5

CB_1R	**Construct**	**pK_i**	**Potency (fold over basal)**	**pK_i**	**Potency (fold over basal)**
	WT	6.2 ± 0.1	1.2 ± 0.1	5.4 ± 0.2	1.3 ± 0.1

H270^{ECL2}L	6.1 ± 0.0	1.4 ± 0.1	5.0 ± 0.4	1.5 ± 0.1
I267^{ECL2}L	6.2 ± 0.1	1.0 ± 0.1	5.9 ± 0.2	1.1 ± 0.0
D266^{ECL2}E	6.4 ± 0.1	1.3 ± 0.1	5.7 ± 0.1	1.5 ± 0.2
Quadruple^{TM1,7}	6.3 ± 0.0	1.6 ± 0.1	5.2 ± 0.0	1.8 ± 0.1*

pEC_{50} <5 was reported when the curve fit was not finished. Values are presented as the mean ± SEM of at least three independent experiments performed in duplicate. One-way Welch ANOVA with Dunnett's T3 posthoc test or Welch's t-test was used to analyze differences in pEC_{50} and E_{max} values compared to WT (*p < 0.05, ** p < 0.01). n.d. not determined.

HU308 and endocannabinoids gain access via membrane entry

The ligand-target binding kinetics (Table 2.2) revealed that the highly lipophilic HU308 and anandamide had a very slow on-rate compared to the other ligands. It has been postulated that ligands of lipid receptors may gain access to the binding pocket via a membrane channel. Both potential ligand entry pathways, *i.e.* either via ECL2 or via a membrane channel between TM1 and TM7, were examined. To this end, four additional mutant receptors were created. Three residues in the ECL2 of CB_2R, which were different from CB_1R, were mutated towards the reciprocal CB_1R residues, i.e. CB_2R-L185^{ECL2}H, CB_2R-L182^{ECL2}I and CB_2R-E181^{ECL2}D. In the fourth mutant receptor, four residues in TM1 and TM7 that align the potential membrane channel in CB_2R were mutated to the reciprocal CB_1R residues and combined as a quadruple mutant, i.e. CB_2R-K279$^{7.33}$T, CB_2R-K33$^{1.32}$Q, CB_2R-V36$^{1.35}$I and CB_2R-C40$^{1.39}$S (termed "CB_2R-Quadruple^{TM1,7}"). Next, all four synthetic agonists and the two endocannabinoids were tested on these four CB_2R mutant receptors in [^{3}H]CP-55,940 and [^{35}S]GTPγS assays. Only CB_2R-L185^{ECL2}H and CB_2R-Quadruple^{TM1,7} were evaluated in the [^{3}H]CP-55,940 displacement assays due to insufficient binding window for the other two mutant receptors (data not shown). The binding affinities of the agonists were not affected for mutant receptors CB_2R-L185^{ECL2}H and CB_2R-Quadruple^{TM1,7} (Table 2.6. Interestingly, the potencies of LEI-102, APD371 and CP-55,940 in the functional assay were not significantly affected for any of the mutant receptors, whereas HU308 and the endocannabinoids were less potent on CB_2R-L182^{ECL2}I (Figure 2.4E-J, Tables 2.4 and 2.6). Additionally, the endocannabinoids showed a decreased potency on CB_2R-L181^{ECL2}D, but not on CB_2R-L185^{ECL2}H. Of note, HU308 and both endocannabinoids completely lost their ability to activate CB_2R in the CB_2R-Quadruple^{TM1,7} mutant, suggesting that this may be an important access point to the receptor binding pocket for these agonists (Figure 2.4G, I-J).

Discussion

Currently, several crystal and cryo-EM CBR structures have been resolved in which non-selective agonists adopt a nearly identical binding position in the orthosteric pocket, regardless of the receptor.[34–38] The results of the site-directed mutagenesis, ligand-target binding kinetics and cryo-EM studies were used to generate a better understanding of the binding and activation mechanism of CB_2R-selective agonists.

F117$^{3.36}$ has an important role in CB_2R activation that does not mimic F200$^{3.36}$ in CB_1R

The data revealed a crucial role for CB_2R-F117$^{3.36}$ as replacement by alanine resulted in a complete loss of G protein activation by all tested agonists (Figure 2.4A-D, Table 2.4). It has been shown that the CB_1R counterpart F200$^{3.36}$ plays an important regulatory role in activation as part of the "twin toggle switch" with CB_1R-W356$^{6.48}$.[39] In contrast, CB_2R-W258$^{6.48}$ has been described to be solely responsible for activation as a toggle switch without the help of CB_2R-F117$^{3.36}$ in structural studies, since the conformation of CB_2R-F117$^{3.36}$ in agonist-bound structures is comparable to the conformation in the antagonist-bound CB_2R structure as well as the CB_1R agonist-bound structures.[33,36] The mutational data supports this hypothesis, as the constitutive activity pattern observed by McAllister *et al.* for the reciprocal CB_1R-F200$^{3.36}$A, is not observed here. This excludes CB_2R-F117$^{3.36}$ from having a suppressive

function.[39] Together, this data provides strong support for a different, but important, role for F117$^{3.36}$ in CB_2R activation.

Potential polar network of H95$^{2.65}$ and S285$^{7.39}$ in CB_2R

In CB_1R, water-mediated interactions between CB_1R-H178$^{2.65}$, CB_1R-S383$^{7.39}$ and bound ligands have previously been shown with *in silico* modelling.[40,41] The importance of CB_1R-S383$^{7.39}$ for classical synthetic cannabinoids such as AM11542, AM841 and CP-55,940 was further emphasized in CB_1R-S383$^{7.39}$A mutants.[36] This is in line with the observation that removal or methylation of the phenolic OH on classical cannabinoids, such as in L-759656, JWH-133 and HU308, always affords selectivity over CB_1R.[18,42] Non-classical agonists, such as WIN55,212-2, do not form a hydrogen bond with CB_1R-S383$^{7.39}$ and consequently are not affected by an alanine mutation.[43] This translates to the observation that CP-55,940 and HU308 are more affected by the CB_2R-S285$^{7.39}$A mutation than LEI-102 and APD371 (Figure 2.4A-D, Table 2.4). The decrease in activation is at least 30-fold smaller for CB_2R than CB_1R.[36] The elucidated cryo-EM structures of the four agonists chosen in this study did not show direct interactions with CB_2R-H95$^{2.65}$, though its role in stabilizing the surrounding residues cannot be ruled out. The large effect seen on G protein activation of CB_2R-H95$^{2.65}$A by LEI-102, APD371 and CP-55,940 (Figure 2.4A-D, Table 2.4) must therefore stem from an indirect interaction, supporting the polar network hypothesis between CB_2R-H95$^{2.65}$ and CB_2R-S285$^{7.39}$ in CB_2R.

V261$^{6.51}$ as a potential selectivity hotspot for CB_2R over CB_1R

Residues at position 6.51 have previously been described to be involved in the binding sites of μ, δ, and κ opioid receptors, the dopamine D2 receptor and adenosine receptors, and could play a role in ligand binding selectivity between different subtypes.[44–46] The results show a reduction of G protein activation by APD371, HU308, and CP-55,940 with introduction of the bulkier CB_1R leucine in CB_2R-V261$^{6.51}$L. LEI-102 could still be accommodated in the binding pocket and was not affected (Figure 2.4A-D, Table 2.4). Additionally, in the swap mutant CB_1R-L359$^{5.61}$V partial recovery of [^{3}H]CP-55,940 replacement was found for CB_2R-selective agonists LEI-102, HU308 and APD371, albeit not significant (Table 2.5). This supports the role of this residue in selectivity of agonists in CB_2R.

The lowly-conserved ECL2 is a large effector of GPCR selectivity

The ECL2 has frequently been implicated to be important for GPCR activation and some GPCRs even use their ECL2 as a ligand to auto-activation.[47] There are distinct differences between the conformations of ECL2 in CB_1R and CB_2R. In antagonist-bound CB_1R crystal structures, the ECL2 dips into the binding pocket, interacting with the ligand and inducing the inactive conformation.[31,32] The inactive state of CB_2R, however, does not expand like CB_1R and instead the ECL2 acts more as a lid on the binding pocket in active and inactive CB_2R, akin to active CB_1R.[33] A key distinction seen in the CB_1R crystal structures with AM6538 and Taranabant, is the ionic lock formed by CB_1R-E100$^{N\text{-terminus}}$ (CB_2R-L17) and CB_1R-H270^{ECL2} (CB_2R-L185).[31,32] The results showed improved binding of [^{3}H]CP-55,940 for LEI-102 and HU308 with the CB_1R-H270^{ECL2}L mutation, while the non-selective agonists showed no change (Table 2.5). Through the loss of this ionic lock, selectivity over CB_1R is partially lost, showing that expulsion of ECL2 upon ligand entry may play an important role in selectivity.

An alternative entry pathway for lipophilic agonists via a membrane channel

In recent years, computational studies have suggested that lipophilic ligands for various GPCRs, such as the opsin receptor, sphingosine-1-phosphate receptor 1 ($S1P_1$) and cannabinoid receptors, might gain access to the binding pocket through lateral diffusion via a membrane channel between TM1 and TM7.[32,40,48–51] The membrane entry pathway was evaluated with a CB_2R quadruple mutant (K33$^{1.32}$Q, V36$^{1.35}$I, C40$^{1.39}$S and K279$^{7.33}$T), which showed a significant loss in potency and a corresponding decrease in affinity, albeit not significant, for HU308 and the endocannabinoids (Figure 2.4E-J, Table 2.4

and 2.6). These compounds are more lipophilic than LEI-102 and APD371, making them more suitable to traverse the membrane to enter between TM1 and TM7. Notably, HU308 and anandamide also showed a substantially longer ET in the kinetic assays compared to the other agonists (Table 2.2). This might suggest a possible relationship between slow association and membrane channel entry at the CB_2R. Likewise, for a peptide GPCR a trend in reduced association rate was found with increasing lipophilicity.[52] Alternatively, this is in contrast with the mechanism at the α2-adrenoceptor at which lipophilic compounds had a faster association rate.[53] This shows the diversity in drug-target binding kinetics as receptor-specific properties and thus the importance of investigating these mechanisms for individual receptors.[54]

The discovery of a membrane access channel for endocannabinoids on the CB_2R is also intriguing from a physiological perspective. Endocannabinoids are produced on demand and act as autocrine or paracrine effectors in the immune system regulating the migration of CB_2R-expressing immune cells.[17] The results suggest that endocannabinoids first have to travel through the plasma membrane via lateral diffusion to reach the receptor. This may suggest that the trafficking and cellular uptake of endocannabinoids could be regulated through extracellular or intracellular vesicles that merge with the plasma membrane. Regardless of the exact mechanism of endocannabinoid trafficking, the results provide experimental evidence of a membrane channel located between TM1 and TM7 in CB_2R that is used by the endocannabinoids to enter the receptor.

Conclusion

In silico and mutational studies on LEI-102 and five other CBR agonists have shown that physicochemical properties determine both pharmacokinetic properties of the ligand and their manner of engagement with the target. The ECL2 and CB_2R-V261$^{5.61}$ are hotspots for inducing selectivity over CB_1R, and CB_2R-F117$^{3.36}$ is vital for receptor activation. Additionally lipophilic ligands including the endocannabinoids may enter the binding pocket through a membrane entrance between TM1 and TM7. Altogether, these discovered molecular mechanisms for selective receptor engagement and activation can have implication for drug design and lipid signaling at GPCRs in general.

Experimental Section

Chemistry

General Remarks

All reagents and solvents were purchased from commercial sources and were of analytical grade (Sigma-Aldrich, BroadPharm®). Reagents and solvents were not further purified before use. All moisture sensitive reactions were performed under inert atmosphere. Solvents were dried using 4 Å molecular sieves prior to use when anhydrous conditions were required. Water used in reactions was always demineralized. Analytical Thin-layer Chromatography (TLC) was routinely performed to monitor the progression of a reaction and was conducted on Merck Silica gel 60 F254 plates. Reaction compounds on the TLC plates were visualized by UV irradiation (λ254) and/or spraying with potassium permanganate solution (K_2CO_3 (40 g), $KMnO_4$ (6 g), and H_2O (600 mL)), ninhydrin solution (ninhydrin (1.5 g), n-butanol (100 mL) and acetic acid (3.0 mL)) or molybdenum solution ($(NH_4)_6Mo_7O_{24}{\cdot}4H_2O$ (25 g/L) and $(NH_4)_4Ce(SO_4)_4{\cdot}2H_2O$ (10 g/L) in sulfuric acid (10%)) followed by heating as appropriate. Purification by flash column chromatography was performed using Screening Devices B.V. silica gel 60 (40-63 µm, pore diameter of 60 Å). Solutions were concentrated using a Heidolph laborata W8 4000 efficient rotary evaporator with a Laboport vacuum pump. Analytical purity was determined with Liquid Chromatography-Mass Spectrometry (LC-MS) using a Finnigan LCQ Advantage MAX apparatus with electrospray ionization (ESI), equipped with a Phenomenex Gemini 3 µm NX-C18 110Å column (50x4.6mm), measuring absorbance at 254 nm using a Waters 2998 PDA UV detector and the m/z ratio by using an Acquity Single Quad (Q1) detector. Injection was with the Finnigan Surveyor Autosampler

Plus and pumped through the column with the Finnigan Surveyor LC pump plus to be analyzed with the Finnigan Surveyor PDA plus detector. Samples were analyzed using eluent gradient 10% → 90% ACN in MilliQ water (+ 0.1% TFA (v/v)). For purification by mass guided preparative High-Performance Liquid Chromatography (Prep-HPLC) was performed on a Waters AutoPurification HPLC/MS apparatus with a Gemini prep column 5 µm 18C 110 Å (150x21.2mm), Waters 2767 Sample manager, Waters 2545 Binary gradient module, Waters SFO System fluidics organizer, Waters 515 HPLC pump M, Waters 515 HPLC pump L attached to a Waters SQ detector Acquity Ultra performance LC. A five column volume purification protocol was applied with the eluents A: 0.2% aq. TFA, B: ACN, flow 25 mL/min, with a minimum start gradients of 0% to maximum end gradient of 100% of B. ^{1}H, ^{13}C, ^{1}H-COSY and HSQC Nuclear Magnetic Resonance (NMR) spectra were recorded on a Bruker AV 300 (300/75 MHz), AV 400 (400/100 MHz) or AV 500 (500/125 MHz) spectrometer at ambient temperature using $CDCl_3$ as solvent. Chemical shifts (δ) are referenced in parts per million (ppm) with tetramethylsilane (TMS) or $CDCl_3$ resonance as the internal standard peak ($CDCl_3$/TMS, δ 0.00 for ^{1}H (TMS), δ 77.16 for ^{13}C ($CDCl_3$)). Multiplicity is reported as bs = broad singlet, s = singlet, d = doublet, bd = broad doublet, dd = doublet of doublet, t = triplet, q = quartet, p = quintet, m = multiplet. Coupling-constants (*J*) are reported in Hertz (Hz).

Synthesis of LEI-102

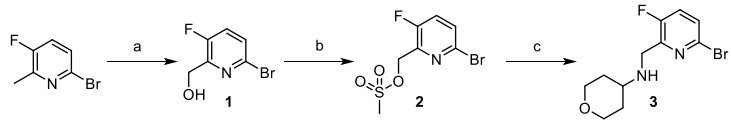

Scheme 2.2 Reagents and conditions: a) Step 1: *m*-CPBA (1.8 eq), 0 °C-RT, DCM, 4 days; Step 2: TFAA (2.2 eq), 55 °C, 3 h; Step 3: K_2CO_3 (2.4 eq), THF:MeOH (20:1), 17 h, 35% (three steps); b) Et_3N (2.3 eq), MsCl (1.7 eq), THF, 0 °C-RT, 1 h, 75%; c) K_2CO_3 (2.2 eq), tetrahydro-2H-pyran-4-amine (1.3 eq), ACN, 50 °C, 3 h, 67%.

(6-Bromo-3-fluoropyridin-2-yl)methanol (1): To a stirred and cooled (0 °C) mixture under inert atmosphere of 6-bromo-3-fluoro-2-methylpyridine (10.7 g, 56.3 mmol, 1 eq) in DCM (370 mL) was added portion-wise *m*-CPBA (23.6 g, 70-75%, 100 mmol, 1.8 eq). The reaction mixture was stirred at room temperature (RT) for 4 days. Sat. $NaHCO_3$ (aq) and sat. $Na_2S_2O_3$ (aq) was added (1:1, v/v) and the layers were separated. The aqueous layer was extracted thrice with DCM. The combined organic layer was dried ($MgSO_4$), filtered, and concentrated under reduced pressure. To the residue was added TFAA (17 mL, 122 mmol, 2.2 eq) at 0 °C. After 15 minutes the temperature was increased to 55 °C for 3 h. The mixture was concentrated under reduced pressure, redissolved in DCM and sat. Na_2CO_3 (aq) was added. The layers were separated and the organic layer was washed with sat. $NaHCO_3$ (aq). The solvent was evaporated and the crude was dissolved in THF:MeOH (20:1, v/v) and K_2CO_3 (18.2 g, 132 mmol, 2.3 eq) was added. After 17 h H_2O was added and the layers were separated. The aqueous layer was extracted thrice with EtOAc. The combined organic layer was dried ($MgSO_4$), filtered, and the solvent evaporated under reduced pressure. The crude product was purified with flash column chromatography (10-20% EtOAc in pentane) to yield a white solid (5.79 g, 19.7 mmol, 35%). ^{1}H-NMR (500 MHz, $CDCl_3$) δ 7.42 (ddt, *J* = 8.5, 3.5, 0.7 Hz, 1H), 7.29 (t, *J* = 8.5 Hz, 1H), 4.80 (d, *J* = 3.3 Hz, 2H). ^{13}C-NMR (126 MHz, $CDCl_3$) δ 156.10 (d, *J* = 256.2 Hz), 148.74 (d, *J* = 19.1 Hz), 135.01 (d, *J* = 2.9 Hz), 128.17 (d, *J* = 4.2 Hz), 126.09 (d, *J* = 19.8 Hz), 59.07.

(6-Bromo-3-fluoropyridin-2-yl)methyl methanesulfonate (2): To a cooled (0 °C) mixture of **1** (1.6 g, 7.8 mmol, 1 eq) and Et_3N (2.5 mL, 17.9 mmol, 2.3 eq) in dry THF (40 mL) was added dropwise MsCl (1.0 mL, 12.9 mmol, 1.7 eq). After stirring at RT for 1 h the solution was concentrated under reduced pressure. DCM and H_2O were added and the layers were separated. The aqueous layer was extracted thrice with DCM. The combined organic layer was washed with brine, dried ($MgSO_4$), filtered, and the

solvent evaporated under reduced pressure to yield a yellow solid (1.65 g, 5.8 mmol, 75%). ^{1}H-NMR (500 MHz, $CDCl_3$) δ 7.52 (dd, *J* = 8.6, 3.5 Hz, 1H), 7.37 (t, *J* = 8.5 Hz, 1H), 5.33 (d, *J* = 2.1 Hz, 2H), 3.13 (s, 3H). ^{13}C-NMR (126 MHz, $CDCl_3$) δ 157.82 (d, *J* = 261.3 Hz), 142.15 (d, *J* = 16.0 Hz), 130.74 (d, *J* = 4.4 Hz), 127.06 (d, *J* = 20.4 Hz), 65.50 (d, *J* = 1.6 Hz), 38.39.

***N*-((6-Bromo-3-fluoropyridin-2-yl)methyl)tetrahydro-2*H*-pyran-4-amine (3)**: A stirred suspension of **2** (1.49 g, 5.3 mmol, 1 eq), K_2CO_3 (1.6 g, 11.6 mmol, 2.2 eq) and tetrahydro-2*H*-pyran-4-amine (0.66 mL, 6.7 mmol, 1.3 eq) in acetonitrile (25 mL) was heated (50 °C) for 6 h, then stirred an additional 3 days at RT. After dilution with DCM and H_2O the layers were separated. The aqueous layer was extracted thrice with DCM. The combined organic layer was dried ($MgSO_4$), filtered, and the solution evaporated under reduced pressure. The crude product was purified with flash column chromatography (20-100% EtOAc in pentane) to yield a yellow oil (1.01 g, 3.5 mmol, 67%). ^{1}H-NMR (300 MHz, $CDCl_3$) δ 7.40 (dd, *J* = 8.6, 3.6 Hz, 1H), 7.35 – 7.26 (m, 1H), 4.08 – 3.95 (m, 4H), 3.42 (td, *J* = 11.6, 2.2 Hz, 2H), 2.74 (tt, *J* = 10.5, 4.1 Hz 1H), 1.89 (ddd, *J* = 12.7, 4.5, 2.3 Hz, 2H), 1.52 (dtd, *J* = 13.1, 11.0, 4.5 Hz, 2H). ^{13}C-NMR (75 MHz, $CDCl_3$) δ 157.12 (d, *J* = 255.9 Hz), 149.21 (d, *J* = 17.0 Hz), 127.83 (d, *J* = 4.2 Hz), 125.97 (d, *J* = 21.2 Hz), 66.76, 53.64, 44.90, 33.59.

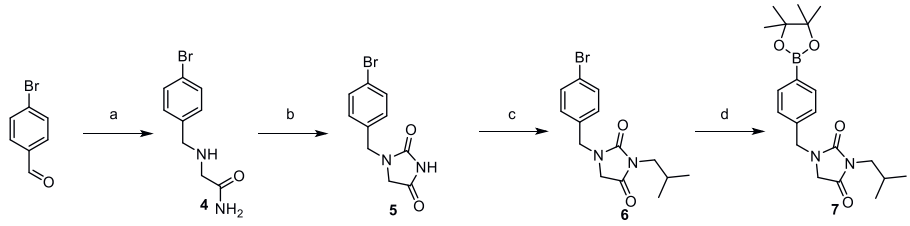

Scheme 2.3 Reagents and Conditions: a) Step 1: 2-aminoacetamide hydrochloride (1.0 eq), NaOH (1.1 eq), MeOH:H_2O (5:1), RT, 18 h; Step 2: $NaBH_4$ (2.1 eq), 18 h, 91% (two steps); b) CDI (2.1 eq), DMAP (2.1 eq), ACN, 60 °C, 70 h, 37%; c) K_2CO_3 (3.0 eq), 1-bromo-2-methylpropane (2.0 eq), DMF, RT, 20 h, 88%; d) KOAc (4.4 eq), bis(pinacolato)diboron (1.5 eq), Pd(dppf)Cl_2 (0.06 eq), DMF, 75 °C, 20 h.

2-((4-Bromobenzyl)amino)acetamide (4): To a stirred mixture of 4-bromobenzaldehyde (9.2 g (49.7 mmol, 1.1 eq) and 2-aminoacetamide hydrochloride (5.06 g, 45.8 mmol, 1.0 eq) in MeOH:H_2O (170 mL, 5:1, v/v) was added NaOH (2.06 g, 51.5 mmol, 1.1 eq). After stirring at RT overnight, $NaBH_4$ (3.6 g, 95.2 mmol, 2.1 eq) was added and the solution was stirred overnight at RT. The solution was acidified to pH 3 with 2 M HCl, then neutralized with sat. $NaHCO_3$ (aq). Methanol was evaporated under reduced pressure and the resulting slurry was filtered to yield a white solid (11.0 g, 45.2 mmol, 91%). ^{1}H-NMR (300 MHz, MeOD) δ 7.69 – 7.59 (m, 2H), 7.47 – 7.38 (m, 2H), 4.22 (s, 2H), 3.81 (s, 2H).

1-(4-Bromobenzyl)imidazolidine-2,4-dione (5): To stirred suspension of **4** (10.0 g, 40.1 mmol, 1.0 eq) in acetonitrile (300 mL) were added CDI (13.86 g, 85.5 mmol, 2.1 eq) and DMAP (10.2 g, 83.5 mmol, 2.1 eq). The mixture was heated (60 °C) under inert atmosphere for 70 h. 1 M HCl (aq, 250 mL) was added and the aqueous layer extracted thrice with EtOAc. The combined organic layer was washed with H_2O and brine, dried ($MgSO_4$), filtered, and the solvent evaporated under reduced pressure. The crude product was purified with flash column chromatography with dry loading over Celite (5-10% acetone in DCM) to yield a yellow solid (3.95 g, 14.7 mmol, 37%). ^{1}H-NMR (300 MHz, $CDCl_3$) δ 7.83 (bs, 1H), 7.56 – 7.45 (m, 2H), 7.20 – 7.10 (m, 2H), 4.49 (s, 2H), 3.79 (s, 2H). ^{13}C-NMR (75 MHz, $CDCl_3$) δ 132.41, 129.95, 77.58, 77.16, 76.74, 50.36, 46.01.

1-(4-Bromobenzyl)-3-isobutylimidazolidine-2,4-dione (6): To a stirred solution of **5** (2.00 g, 7.4 mmol, 1,0 eq) in anhydrous DMF (18 mL) were subsequently added K_2CO_3 (3.08 g, 22.3 mmol, 3,0 eq) and 1-bromo-2-methylpropane (1.62 mL, 14.9 mmol, 2,0 eq). After stirring at RT for 20 h, the mixture was

filtered and the filtrate diluted with diethyl ether and washed thrice with H_2O (3 x 50 mL). The combined organic layer was washed with brine, dried ($MgSO_4$), filtered, and concentrated under reduced pressure. The crude product was purified with flash column chromatography (10-40% EtOAc in pentane) to yield a white solid (2.12 g, 6.52 mmol, 88%). ^{1}H-NMR (300 MHz, $CDCl_3$) δ 7.47 (d, *J* = 8.3 Hz, 2H), 7.14 (d, *J* = 8.3 Hz, 2H), 4.52 (s, 2H), 3.74 (s, 2H), 3.33 (d, *J* = 7.4 Hz, 2H), 2.15 – 2.04 (m, 1H), 0.91 (d, *J* = 6.8 Hz, 6H). ^{13}C-NMR (75 MHz, $CDCl_3$) δ 169.57, 156.78, 134.41, 131.79, 129.48, 121.77, 60.01, 48.61, 45.98, 45.71, 28.57, 19.70. LCMS (LCQ Fleet, 10-90): t_r = 7.00 min, m/z: 325.17 $[M+H]^+$, 327.08 $[M+H]^+$ (Br).

3-Isobutyl-1-(4-(4,4,5,5-tetramethyl-1,3,2-dioxaborolan-2-yl)benzyl)imidazolidine-2,4-dione (7): A mixture of **6** (0.50 g, 1.54 mmol, 1 eq), KOAc (0.66 g, 6.76 mmol, 4.4 eq) and bis(pinacolato)diboron (0.59 g, 2.31 mmol, 1.5 eq) in DMF (10 mL) was sonicated for 15 min under argon flow. Subsequently, $Pd(dppf)Cl_2$ (0.07 g, 0.09 mmol, 0.06 eq) was added and the mixture was heated (75 °C) for 20 h. The mixture was cooled to RT, diluted with EtOAc (100 mL) and H_2O (10 mL) and the layers were separated. The aqueous layer was extracted thrice with EtOAc (3 × 20 mL). The combined organic layer was extracted with sat. $NaHCO_3$ (aq), H_2O and brine, dried ($MgSO_4$), filtered, and concentrated under reduced pressure. The crude product was co-evaporated with $CHCl_3$ and used in the next step without further purification.

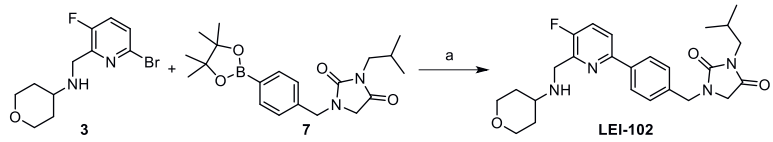

Scheme 2.4 Reagents and Conditions: a) **3** (1.0 eq), **7** (1.5 eq), K_2CO_3 (6.0 eq), $Pd(PPh_3)_4$ (0.1 eq), toluene:EtOH (4:1), 75 °C, 18 h, 45% (two steps).

1-(4-(5-Fluoro-6-(((tetrahydro-2H-pyran-4-yl)amino)methyl)pyridin-2-yl)benzyl)-3-isobutylimidazolidine-2,4-dione (LEI-102): To a degassed mixture of **3** (0.29 g, 1.0 mmol, 1,0 eq), **7** (0.56 g, ~1.5 mmol, crude) and K_2CO_3 (1.29 g, 6.0 mmol, 6,0 eq) in toluene:ethanol (10 mL, 4:1, v/v) was added under argon atmosphere $Pd(PPh_3)_4$ (0.18 g, 0.10 mmol, 0.1 eq). The resulting mixture was heated (75° for 18 h, then cooled to RT and filtered. The filtrate was diluted with EtOAc and washed with H_2O and brine, dried ($MgSO_4$), filtered, and concentrated under reduced pressure. The crude product was purified with flash column chromatography (0-20% MeOH in EtOAc) to yield a white solid (0.24 g, 0.53 mmol, 53%). Further purification with preparative HPLC resulted in a yield of 0.204 g (0.45 mmol, 45%). ^{1}H-NMR (400 MHz, CD_3CN) δ 8.05 (d, *J* = 8.3 Hz, 2H), 7.86 (dd, *J* = 8.7, 3.6 Hz, 1H), 7.61 (t, *J* = 9.0 Hz, 1H), 7.34 (d, *J* = 8.1 Hz, 2H), 4.53 (s, 2H), 4.45 (s, 2H), 3.93 (dd, *J* = 11.4, 4.4 Hz, 2H), 3.77 (s, 1H), 3.47 (tt, *J* = 11.8, 3.8 Hz, 2H), 3.30 (td, *J* = 11.9, 1.9 Hz, 2H), 3.24 (d, *J* = 7.3 Hz, 2H), 2.05 (bd, *J* = 13.3 Hz, 2H), 1.99 (dt, *J* = 13.2, 6.6 Hz, 1H), 1.83 (qd, *J* = 12.1, 4.5 Hz, 2H), 0.88 (d, *J* = 6.7 Hz, 6H). ^{13}C-NMR (100 MHz, CD_3CN) δ 171.54, 157.25 (d, *J* = 226.6 Hz), 156.12, 153.03 (d, *J* = 4.5 Hz), 140.51 (d, *J* = 16.1 Hz), 138.83, 137.70, 129.13, 128.22, 125.56 (d, *J* = 18.8 Hz), 122.81 (d, *J* = 4.3 Hz), 118.38, 66.55, 55.55, 50.30, 46.81 (d, *J* = 7.9 Hz), 42.95, 30.02, 28.32, 20.32. LCMS (LCQ Advantage, 10 90%): t_r = 5.32 min, m/z: 455.27 $[M+H]^+$, 908.93 $[2M+H]^+$. HRMS (ESI+) m/z: calcd. for $C_{25}H_{32}FN_4O_3$ [M+H], 455.245; found, 455.245.

Biology

General Remarks

Monoclonal M2 mouse anti-FLAG primary antibody (#F3165) was purchased from Sigma-Aldrich (Zwijndrecht, the Netherlands), while secondary goat anti-mouse HRP-conjugated antibody (#115-035-003) was bought from Jackson ImmunoResearch Laboratories (West Grove, PA, USA). Bicinchoninic acid

(BCA) ad BCA protein assay reagent was obtained from Pierce Chemical Company (Rockford, IL, USA). [^{3}H]-RO6957022 (specific activity 82.83 Ci mmol^{-1}) was custom synthesized at F. Hoffman-La Roche Ltd (Basel, Switzerland). [^{35}S]GTPγS (specific activity 1250 Ci mmol^{-1} #NEG030H250UC), [^{3}H]-CP-55,940 (specific activity 108.5 Ci mmol^{-1} #NET1051250UC) and GF/C filter plates (#6055690) were purchased from PerkinElmer (Waltham, MA, USA). CP-55,940 (#C1112), AM630 (#SML0327) and DL-dithiotreitol (DTT, #646563) were obtained from Sigma-Aldrich, HU308 (#H800010) was from LKT Laboratories (St. Paul, MN, USA), APD371 was provided by F. Hoffmann-La Roche Ltd, anandamide (AEA, #1339), 2-Arachidonylglycerol (2-AG, #1298) and phenylmethylsulfonyl fluoride (PMSF, #4486) were purchased from Tocris Bioscience (Bristol, UK) and GDP (#J61646) was from Thermo Fisher Scientific (Waltham, MA, USA). All buffers and solutions were prepared using Millipore water (deionized using a MilliQ A10 Biocel with a 0.22 µm filter) and analytical grade reagents and solvents. Buffers are prepared at room temperature (RT) and stored at 4 °C, unless stated otherwise.

Quantification and statistical analysis

All experimental data were analyzed using GraphPad Prism 9.0 (GraphPad Software Inc., San Diego, CA). All values obtained are means ± standard error of the mean (SEM) of at least three independent experiments performed in duplicate, unless stated otherwise.

From [^{3}H]-RO6957022 competition association assays, the k_{on} and k_{off} were determined by non-linear regression analysis, using the "kinetics of competitive binding" model as described by Motulsky and Mahan[55]:

$$K_a = k_1 \cdot [L] \cdot 10^{-9} + k_2$$

$$K_b = k_3 \cdot [I] \cdot 10^{-9} + k_4$$

$$S = \sqrt{(K_a - K_b)^2 + 4 \cdot k_1 \cdot k_3 \cdot [L] \cdot [I] \cdot 10^{-18}}$$

$$K_f = 0.5 \cdot (K_a + K_b + S)$$

$$K_s = 0.5 \cdot (K_a + K_b - S)$$

$$Q = \frac{Bmax \cdot k_1 \cdot [L] \cdot 10^{-9}}{K_f - K_s}$$

$$[Y] = Q \cdot \left(\frac{k_4 \cdot (K_f - K_s)}{K_f \cdot K_s} + \frac{k_4 - K_f}{K_f} \cdot \mathrm{e}^{(-K_f \cdot X)} - \frac{k_4 - K_s}{K_s} \cdot \mathrm{e}^{(-K_S \cdot X)} \right)$$

Where [L] is the radioligand concentration per experiment (~1.5 nM), I is the IC_{50} concentration of agonist (nM), X is the time (s), and Y is the specific binding of the radioligand (dpm). K_a and K_b are the observed association rate constants (k_{obs}) of the radioligand and the agonist of interest, respectively. k_1 and k_3 are the association rate constants (k_{on} in $M^{-1}s^{-1}$) of [^{3}H]-RO6957022 (determined per experiment) and the agonist of interest, respectively. Similarly, k_2 and k_4 are the dissociation rate constants (k_{off} in s^{-1}) of [^{3}H]-RO6957022 (experimentally determined at 4.3×10^{-4} s^{-1}, data not shown) and the agonist of interest, respectively. The engagement time (ET in seconds) of the agonists of interest was determined at 1 µM of agonist using the equation ET= $1/(k_{on} \cdot 1 \times 10^{-6})$. The residence time distribution (RTD in min) was calculated using the equation RTD=$1/(60 \cdot k_{off})$.[56] The association and dissociation rate constants were used to calculate the kinetic K_D using: $K_D = k_{off}/k_{on}$.

[^{35}S]GTPγS agonist responses on CB_2R constructs were baseline-corrected for the individual mutant's basal activity. The responses were normalized to the basal activity of the construct (0%) and top of the CP-55,940 (for WT responses only) or WT curve (for mutants, 100%). The potency (pEC_{50}) and efficacy (E_{max}) values were obtained by non-linear regression to a sigmoidal concentration-effect curve with a

Hill slope of 1 by using the "log(agonist) vs response (three parameters)" model. [^{35}S]GTPγS data from CB_1R constructs were expressed as fold over the mutant's basal activity to also quantify the effects of CB_2R selective agonists.

Displacement assays were baseline-corrected with NSB and normalized to this value (0%) and TB (100%). The equilibrium dissociation constants (K_D) of [^{3}H]-CP-55,940 on different mutants were calculated from homologous displacements by non-linear regression analysis, using the "one-site homologous" model. The half-maximal inhibitory concentrations (pIC_{50}) of the agonists in [^{3}H]-CP-55,940 and [^{3}H]-RO6957022 assays were obtained by non-linear regression analysis of the homologous and heterologous displacement curves and further converted into inhibitory constant pK_i using the Cheng-Prusoff equation.[57] In which the experimentally determined K_D for each construct was used for [^{3}H]-CP-55,940 assays or 0.78 nM for [^{3}H]-RO6957022 assays (data not shown).

Differences in pEC_{50}, E_{max}, pK_D and pK_i values for each mutant compared to WT were analyzed using a one-way Welch's ANOVA with Dunnett's T3 multiple comparisons test or an unpaired Student's t-test with Welch's correction. Significant differences are displayed as * $p < 0.05$; ** $p < 0.01$, *** $p < 0.001$ and **** $p < 0.0001$.

Cell Culture

Cells were cultured and prepared similar to previously described.[44] Spodoptera frugiperda (Sf9) cells were used for CB2R-Gi co-expression for cryo-EM studies. Sf9 cells were grown in ESF 921 medium (Expression systems) at 27 °C and 125 rpm. For transfections, human embryonic kidney 293 T (HEK293T; female, ATCC #CRL-3216) cells were grown as monolayers in culture medium i.e. Dulbecco's Modified Eagle's Medium (Sigma-Aldrich #6546), supplemented with 10% fetal calf serum (Sigma-Aldrich #F7524), 2 mM L-glutamine (Sigma-Aldrich #G8541), 100 IU/mL penicillin and 100 µg/mL streptomycin (Duchefa Biochemie #P0142 and #S0148) under a humidified atmosphere at 37 °C with 5% CO_2. Subculture was done twice a week at 80 – 90% confluence on 10 cm ø plates by trypsinization. CHO cells stably expressing hCB_2 (CHOK1_hCB_2R_bgal; PathHunter EA Parental Cell line, female, DiscoverX #93-0706C2) were cultured in Ham's F12 Nutrient Mixture (Sigma-Aldrich #4888) supplemented with 10% fetal calf serum, 2 mM L-glutamine, 100 IU/mL penicillin, 100 µg/mL streptomycin, 300 µg/mL hygromycin (Bio-Connect #ANT-HG-5) and 800 µg/mL G418 (Bio-Connect #SC-29065B) in a humidified atmosphere at 37 °C with 5% CO_2. Cells were subcultured twice a week when reaching 80 - 90% confluence on 10 or 15 cm ø plates by trypsinization.

Constructs and Expression of CB_2R and G_i heterotrimer

A N-BRIL fused WT human CB_2R construct was cloned into a modified pFastBac1 vector with an HA signal sequence at the N-terminus followed by a 10×His-tag and a FLAG-tag. Human $G_{\alpha i1}$ and $G_{\beta 1\gamma 2}$ subunits were cloned into pFastbac1 and pFastDual vector individually. The CB_2R and G_i heterotrimer were co-expressed in Sf9 insect cells using the Bac-to-Bac Baculovirus Expression System (Invitrogen). Sf9 cells were infected at a cell density of 2-2.5×10^6 cells/ml with three separate virus preparations for CB_2R, $G_{\alpha i1}$ and $G_{\beta 1\gamma 2}$ at a ratio of 1:2:2. The infected cells were cultured at 27 °C for 48 h before collection by centrifugation and the cell pellets were stored at -80 °C for future use.

Constructs, Expression and Purification of scFv16

Methods of complex expression and purification in the current study have been described previously.[34] The CB_2R and G_i heterotrimer were co-expressed in Sf9 insect cells using the Bac-to-Bac Baculovirus Expression System (Invitrogen). Cells were infected with three separate virus preparations for CB_2R, $G_{\alpha i1}$ and $G\beta_{1\gamma 2}$ at a ratio of 1:2:2 at a cell density of 2.5×10^6 cells/mL. After 48 h, the cell culture was collected by centrifugation and the cell pellets were stored at -80 °C until use. The cell pellets were thawed and lysed in the hypotonic buffer of 10 mM HEPES (pH 7.5), 10 mM $MgCl_2$, 20 mM KCl with EDTA-free

complete protease inhibitor cocktail tablets (Roche, #5056489001). The CB_2R-G_i complex was formed in membranes by addition of 25 µM agonist (LEI-102, APD371, HU308 and CP-55,940, respectively) and 2 units of apyrase (NEB, #M0398S) in the presence 500 µg scFv16. The lysate was incubated for overnight at 4 °C and discard the supernatant by centrifugation at 40,000 rpm for 30 min. Subsequently, the solubilization buffer containing 50 mM HEPES (pH 7.5), 100 mM NaCl, 0.75% (w/v) lauryl maltose neopentyl glycol (LMNG, Anatrace, #4216588), 0.15% (w/v) cholesterol hemisucinate (CHS, Sigma-Aldrich, #C6512) supplemented with 25 µM agonist and 2 units of apyrase (NEB) were added to solubilize complexes for 2 h at 4 °C. Insoluble material was removed by centrifugation at 40,000 rpm for 30 min and the supernatant was immobilized by batch binding to TALON IMAC resin (Clontech, #635507) including 20 mM imidazole over 6 h at 4 °C. Then, the resin was packed and washed with 15 column volumes (CVs) of washing buffer I containing 25 mM HEPES (pH 7.5), 100 mM NaCl, 10% (v/v) glycerol, 0.1% (w/v) LMNG, 0.02% (w/v) CHS, 30 mM imidazole and 20 µM agonist, and 15 CVs of washing buffer II containing 25 mM HEPES (pH 7.5), 100 mM NaCl, 10% (v/v) glycerol, 0.03% (w/v) LMNG, 0.006% (w/v) CHS, 50 mM imidazole and 20 µM agonist. After that, the protein was eluted using 3 CVs of elution buffer containing 25 mM HEPES (pH 7.5), 100 mM NaCl, 10% (v/v) glycerol, 0.01% (w/v) LMNG, 0.002% (w/v) CHS, 250 mM imidazole and 25 µM agonist. Finally, the complex was concentrated using the centrifugal filter with 100 KD molecular weight cutoff and loaded onto a Superdex200 10/300 GL column (GE Healthcare) with buffer containing 20 mM HEPES (pH 7.5), 100 mM NaCl, 0.00075% (w/v) LMNG, 0.00025% GDN (Anatrace, #GDN101), 0.0001% (w/v) CHS, 100 µM TCEP. The fractions consisting of purified CB_2-G_i complex were collected and concentrated to 0.8-1.0 mg/ml for electron microscopy experiments.

CB_2R-G_i-scFv16 Complex Formation and Purification

The cell pellets corresponding to 1 L CB_2R-G_i co-expression culture were thawed and lysed in the hypotonic buffer of 10 mM HEPES, pH7.5, 10 mM $MgCl_2$, 20 mM KCl with EDTA-free complete protease inhibitor cocktail tablets (Roche). The CB_2R-G_i complex was formed in membranes by addition of 20 µM agonist (LEI-102, APD371, HU308 or CP-55,940) and 2 units of apyrase (NEB) in the presence of 500 µg scFv16. The lysate was incubated overnight at 4 °C and the supernatant discarded after centrifugation at 40,000 rpm for 30 min. The complex was separated from the membranes in buffer containing 50 mM HEPES (pH 7.5), 100 mM NaCl, 0.75% (w/v) lauryl maltose neopentyl glycol (LMNG, Anatrace), 0.15% (w/v) cholesterol hemisucinate (CHS, Sigma-Aldrich), 20 µM agonist and 2 units of apyrase (NEB) at 4 °C for 2 h. The supernatant was isolated by ultracentrifugation, and then incubated with TALON IMAC resin (Clontech) and 20 mM imidazole over 6 h at 4 °C. The resin was washed with 15 column volumes of washing buffer I (25 mM HEPES (pH 7.5), 100 mM NaCl, 10% (v/v) glycerol, 0.1% (w/v) LMNG, 0.02% (w/v) CHS, 30 mM imidazole and 20 µM agonist) and 15 column volumes of washing buffer II (25 mM HEPES (pH 7.5), 100 mM NaCl, 10% (v/v) glycerol, 0.03% (w/v) LMNG, 0.006% (w/v) CHS, 50 mM imidazole and 20 µM agonist). The protein was eluted using 3 column volumes of elution buffer (25 mM HEPES (pH 7.5), 100 mM NaCl, 10% (v/v) glycerol, 0.01% (w/v) LMNG, 0.002% (w/v) CHS, 250 mM imidazole and 25 µM agonist). The purified CB_2R-G_i-scFv16 complex was concentrated, then injected onto a Superdex200 10/300 GL column (GE Healthcare) equilibrated in buffer (20 mM HEPES (pH 7.5), 100 mM NaCl, 0.00075% (w/v) LMNG, 0.00025% GDN, 0.0001% (w/v) CHS, 100 µM TCEP). The complex peak fractions were collected and concentrated individually to 0.8-1.0 mg/mL for electron microscopy experiments.

Cryo-EM grid Preparation and data collection

For cryo-EM grids preparation of the CB_2R-G_i complexes, 3 µL of the concentrated protein was loaded to a glow-discharged holey carbon grid (CryoMatrix Amorphous alloy film R1.2/1.3, 300 mesh), and subsequently were plunge-frozen in liquid ethane using a Vitrobot Mark IV (Thermo Fisher Scientific).

The chamber of Vitrobot was set to 100% humidity at 4 °C. The sample was blotted for 2.5 s with blot force 2. Cryo-EM images were collected on a Titan Krios microscope operated at 300 kV equipped with a Gatan Quantum energy filter, with a slit width of 20 eV, a Gatan K2 summit direct electron camera (Gatan). Images were taken at a dose rate of 8e-/Å2/s with a defocus range of -0.8 to -2.0 µm using SerialEM software[58] in EFTEM nanoprobe mode, with 50 µm C2 aperture, at a calibrated magnification of 130,000 corresponding to a magnified pixel size of 1.04 Å. The total exposure time was 8.1 s and 45 frames were recorded per micrograph.

Image Processing and 3D Reconstruction

The cryo-EM data processing was performed with CryoSPARC.[59] For CB_2R-$G_{\alpha i}$-scFv16-APD371/LEI-102/HU308/CP-55,940 dataset, a total of 7443, 5282, 7530 and 6473 movies were collected, respectively. For all datasets, patch motion correction was used for beam-induced motion correction. Contrast transfer function (CTF) parameters for each micrograph were determined by patch CTF estimation. Using Blob Picker in CryoSPARC to auto pick particles in the first 500 micrographs of CB_2R-$G_{\alpha i}$-scFv16-APD371 complex dataset and then 258347 particles were extracted to conduct 2D classification. 9277 particles in good 2D patterns were selected as templates to pick better particles. 5,239,870, 3,398,611, 4,653,294 and 3,595,875 particles extracted, respectively, in a 256 Å box were divided into three hundred two-dimensional (2D) class averages with a maximum alignment resolution of 6 Å. Then, 1,152,146, 762,471, 355,832 and 440,292 particles were selected from good 2D classification after two round 2D classification, individually. Following 2D classification, these particles were subjected for ab initio reconstruction into four classes. After heterogeneous refinement, homogeneous refinement, non-uniform refinement and local refinement of the best-looking dataset in CryoSPARC, the final map has an indicated global resolution of 3.08 Å, 2.98 Å, 2.97 Å and 2.84 Å at a Fourier shell correlation (FSC) of 0.143, respectively. Local resolution was determined using the Bsoft package with half maps as input maps.[60]

Model Building and Refinement

The CB_2R-AM12033 cryo-EM structure and G_i protein in CB_2R were used as the starting model for model refinement. The model was docked into the CB_2R-agonist-G_i-scFv16 EM density map using Chimera[61], followed by iterative manual adjustment and rebuilding in COOT[62] and phenix.real_space_refine in Phenix.[63] The model statistics were validates using MolProbity.[64] Structural figures were prepared in Chimera and PyMOL (http://www.pymol.org). The extent of any model overfitting during refinement was measured by refining the final model against one of the half-maps and by comparing the resulting map versus model FSC curves with the two half-maps and full model.

Generation of Mutants

The WT CB_1R and CB_2R genes were subcloned into vector pcDNA3.1 with an N-terminal HA signal peptide and FLAG-tag. Mutations were introduced by QuikChange PCR (as described by supplier).

Transfection

24 h prior to transfection, HEK293T cells were seeded on 10 cm ø plates to reach approximately 50% confluence at the start of transfection. The cells were transfected with 10 µg plasmid DNA of WT hCB_2R or hCB_1R receptor, or mutant receptor using the calcium phosphate precipitation method.[65] In short, a DNA-calcium mix was made containing 270 mM $CaCl_2$ and 10 µg plasmid DNA to which Hank's Balanced Salt Solution (HBSS; 280 mM NaCl, 10 mM KCl, 1.5 mM Na_2HPO_4 and 50 mM HEPES) was added in a 1:1 (v/v) ratio and mixed by aeration to create consistent calcium phosphate precipitates. For transfection, 1 mL DNA-calcium mix was added per 10 cm ø plate, followed by a 24/48 h incubation under a humidified atmosphere at 37 °C with 5% CO_2.

Enzyme-Linked Immunosorbent Assay (ELISA)

Receptor expression after transfection was measured with ELISA. A control was made by transfecting HEK293T cells transfected with an empty pcDNA3.1 vector. HEK293T cells were transfected 24 h prior to seeding. A clear, culture-treated 96-wells plate was treated with 100 µL/well 0.1 mg/mL poly-D-lysine for 30 min. after which the wells were washed twice with 200 µL/well PBS and the plate air-dried for 1 h. Cells were detached by incubation for 15 min. at 37 °C with 1.5 mL warm PBS/EDTA. 3 mL medium (DMEM, D6546 Sigma Aldrich) was added, cells resuspended and centrifuged at 200 x g for 5 min. The supernatant was aspirated and cells resuspended in medium to 1,000,000 cells/mL. 100 µL is added to each well so that a total of 100,000 cells have been seeded per well.

24 h after seeding the plate was aspirated and washed with 200 µL PBS/well. The cells were fixed with 100 µL/well 4% formaldehyde for 10 min. Then washed twice with 100 µL/well Tris-buffered saline (TBS). The plate was incubated with 100 µL/well blocking buffer (2% (w/v) BSA in TBST) for 30 minutes at 400 rpm. The blocking buffer was aspirated and the plate was incubated with 100 µL/well mouse anti-FLAG primary antibody (1 µg/mL, Sigma F3165) for 2 h at 400 rpm. The antibody was aspirated and after washing thrice with 200 µL/well TBST prior to addition of goat anti-mouse HRP-conjugated secondary antibody (1:10,000 dilution. Jackson ImmunoResearch Laboratories 115-035-003) and 1 h incubation at 400 rpm. The plate was aspirated and washed thrice with 200 µL/well TBS. The plate was incubated with 100 µL/well TMB in the dark for 10 min. until the reaction was quenched with 100 µL 1 M H_3PO_4. Absorbance was measured at 450 nm with the Wallac EnVisionTM (Perking Elmer).

Membrane Preparation

For membrane preparation, HEK293T cells were harvested 48 h after transfection. Cells were detached by scraping into 3 mL of phosphate-buffered saline (PBS) and subsequently centrifuged at 2000 x g for 5 min. Pellets were resuspended in ice-cold Tris buffer (50 mM Tris-HCl, pH 7.4) and homogenized with an Ultra Turrax homogenizer (IKA-Werke GmbH & Co. KG, Staufen, Germany). Cytosolic and membrane fractions were separated using a high-speed centrifugation step of 31,000 rpm in a Beckman Optima LE-80K ultracentrifuge with Ti70 Rotor for 20 min at 4 °C. After a second cycle of homogenization and centrifugation, the final pellets were resuspended in 50 mM Tris-HCl (pH 7.4), 5 mM $MgCl_2$ and stored in 100 µL aliquots at -80 °C until use. CHOK1_hCB_2R_bgal cells were harvested when reaching 90% confluence in 15 cm ø plates after one week subculture at a 1:6 ratio. Membrane preparation followed a similar procedure as described above. Final membrane pellets were resuspended in 50 mM Tris-HCl (pH 7.4) and stored in 100 µL aliquots at -80 °C until use. Membrane protein concentrations were determined using a BCA protein determination assay as described by the manufacturer (Smith et al., 1985).

[^{3}H]-RO6957022 Competition Association Assays

Prior to kinetic assessment of agonist binding, the affinity (IC_{50}) of the agonists at the hCB_2R was determined in [^{3}H]-RO6957022 displacement assays. CHOK1_hCB_2R_bgal was thawed, homogenized, and subsequently diluted to 1 µg protein per well. When studying endocannabinoids, membranes were preincubated with 50 µM PMSF for 30 minutes. Membranes were incubated with ~1.5 nM [^{3}H]-RO6957022 and six increasing concentrations of competing agonists in a total volume of 100 µL assay buffer (50 mM Tris-HCl (pH 7.4), 0.1% (w/v) BSA). Incubations were done for 2 h at 10 °C to reach equilibrium. Subsequently, in competition association assays, agonists were incubated at their IC_{50} concentration in the presence of ~1.5 nM [^{3}H]-RO6957022 in a total volume of 100 µL assay buffer at 10 °C. Competition was initiated by addition of membrane homogenates at different time points for 2 h. Non-specific binding was determined with 10 µM AM630. Organic solvent (DMSO or acetonitrile) concentrations were <1% in all samples. Incubations were terminated by rapid vacuum filtration with ice-cold 50 mM Tris-HCl (pH 7.4), 0.1% (w/v) BSA buffer through Whatman GF/C filters using a

Filtermate 96-well harvester (PerkinElmer). Filters were dried for at least 30 min at 55 °C and subsequently 25 µL MicroScint scintillation cocktail was added per well. Filter-bound radioactivity was measured by scintillation spectrometry using a Microbeta2 2450 counter (PerkinElmer).

[^{35}S]GTPγS Binding Assays

G protein activation was measured with agonists LEI-102, APD371, HU308, CP-55,940 AEA and 2-AG. Transient HEK293T membrane homogenates (10 µg/well) were diluted in assay buffer (50 mM Tris-HCl (pH 7.4), 5 mM $MgCl_2$, 150 mM NaCl, 1 mM EDTA, 0.05% BSA (w/v) and 1 mM DTT) and pretreated with 10 µg saponin and 1 µM GDP. For endocannabinoid samples, the membranes were additionally pretreated for 30 minutes with 50 µM phenylmethylsulfonyl fluoride (PMSF) before agonist addition. The membranes were incubated with 10 µM CP-55,940 (E_{max}) or six increasing concentrations of agonist (ranging from 0.01 nM to 1 µM) for 30 minutes at rt. Basal receptor activity was determined in the presence of vehicle only (0.2% DMSO/acetonitrile). [^{35}S]GTPγS (0.3 nM) was added for 100 µL final volume. The mixture was co-incubated for 90 minutes at 25 °C while shaking at 400 rpm. The plate was filtered with wash buffer (50 mM Tris-HCl (pH 7.4), 0.1% (w/v) BSA) through Whatman GF/C filters using a Filtermate 96-well harvester (PerkinElmer). Filters were dried for at least 30 min at 55 °C and subsequently 25 µL MicroScint scintillation cocktail was added per well. Filter-bound radioactivity was measured by scintillation spectrometry using a Microbeta2 2450 counter (PerkinElmer).

[^{3}H]-CP-55,940 Homologous and Heterologous Displacement Assays

To determine agonist affinity (K_i) on WT and mutant receptors. The amount of transient HEK293T membrane was 0.75 µg to 10 µg protein per well, chosen to reach a specific [^{3}H]-CP-55,940 binding window of 1200-1500 disintegrations per minute (dpm). Only the CB_2R-quadruple mutant was used with 20 µg/well for a window of ~500 dpm. Membranes were thawed and subsequently homogenized using an Ultra Turrax homogenizer. For AEA and 2-AG the membranes were preincubated for 30 minutes with 50 µM PMSF. Homologous displacement assays were performed with 1.5 nM final concentration [^{3}H]-CP-55,940 against six increasing concentrations (0.1 nM to 10 µM) of cold CP-55,940. Heterologous displacement assays were done with LEI-102, APD371, HU308, AEA and 2-AG using 1.5 nM final concentration [^{3}H]-CP-55,940 with one concentration (10 µM) or six increasing concentrations (ranging from 0.1 nM to 10 µM) in assay buffer. To a 96-well roundbottom plate was added 25 µL assay buffer, 25 uL agonist (or buffer for negative control), 25 uL 6 nM [^{3}H]-CP-55,940, and 25 uL membrane, in order. Incubation was for 2 h at 25 °C. Separation of bound from free radioligand was performed by rapid filtration through GF/C filters (Whatman, Clifton, NJ) using a Filtermate Harvester (Brandel Inc., Gaithersburg, MD). Filters were dried for at least 30 min at 55 °C and subsequently 25 µL MicroScint scintillation cocktail was added per well. Filter-bound radioactivity was measured by scintillation spectrometry using a Microbeta2 2450 counter (PerkinElmer).

References

1. Mechoulam R, Hanuš LO, Pertwee R, Howlett AC. Early phytocannabinoid chemistry to endocannabinoids and beyond. *Nat Rev Neurosci*. 2014;15(11):757-764. doi:10.1038/nrn3811

2. Pacher P, Bátkai S, Kunos G. The Endocannabinoid System as an Emerging Target of Pharmacotherapy. *Pharmacol Rev*. 2006;58(3):389-462. doi:10.1124/pr.58.3.2

3. Badowski M, Yanful PK. Dronabinol oral solution in the management of anorexia and weight loss in AIDS and cancer. *Ther Clin Risk Manag*. 2018;Volume 14:643-651. doi:10.2147/TCRM.S126849

4. Grimison P, Mersiades A, Kirby A, et al. Oral THC:CBD cannabis extract for refractory chemotherapy-induced nausea and vomiting: a randomised, placebo-controlled, phase II crossover trial. *Ann Oncol*. 2020;31(11):1553-1560. doi:10.1016/j.annonc.2020.07.020

5. Inglet S, Winter B, Yost SE, et al. Clinical Data for the Use of Cannabis-Based Treatments: A Comprehensive Review of the Literature. *Ann Pharmacother*. 2020;54(11):1109-1143. doi:10.1177/1060028020930189

6. Jones É, Vlachou S. A Critical Review of the Role of the Cannabinoid Compounds Δ9-Tetrahydrocannabinol (Δ9-THC) and Cannabidiol (CBD) and their Combination in Multiple Sclerosis Treatment. *Molecules*. 2020;25(21):4930. doi:10.3390/molecules25214930

7. Adams IB, Martin BR. Cannabis: pharmacology and toxicology in animals and humans. *Addiction*. 1996;91(11):1585-1614. http://www.ncbi.nlm.nih.gov/pubmed/8972919.

8. Lucas CJ, Galettis P, Schneider J. The pharmacokinetics and the pharmacodynamics of cannabinoids. *Br J Clin Pharmacol*. 2018;84(11):2477-2482. doi:10.1111/bcp.13710

9. Pacher P, Steffens S, Haskó G, Schindler TH, Kunos G. Cardiovascular effects of marijuana and synthetic cannabinoids: the good, the bad, and the ugly. *Nat Rev Cardiol*. 2018;15(3):151-166. doi:10.1038/nrcardio.2017.130

10. Riera R, Pacheco RL, Bagattini ÂM, Martimbianco ALC. Efficacy and safety of therapeutic use of cannabis derivatives and their synthetic analogs: Overview of systematic reviews. *Phyther Res*. 2022;36(1):5-21. doi:10.1002/ptr.7263

11. Munro S, Thomas KL, Abu-Shaar M. Molecular characterization of a peripheral receptor for cannabinoids. *Nature*. 1993;365(6441):61-65. doi:10.1038/365061a0

12. Howlett AC. International Union of Pharmacology. XXVII. Classification of Cannabinoid Receptors. *Pharmacol Rev*. 2002;54(2):161-202. doi:10.1124/pr.54.2.161

13. Pertwee RG, Howlett AC, Abood ME, et al. International Union of Basic and Clinical Pharmacology. LXXIX. Cannabinoid Receptors and Their Ligands: Beyond CB 1 and CB 2. *Pharmacol Rev*. 2010;62(4):588-631. doi:10.1124/pr.110.003004

14. Howlett AC, Abood ME. CB 1 and CB 2 Receptor Pharmacology. In: ; 2017:169-206. doi:10.1016/bs.apha.2017.03.007

15. Howlett A, Blume L, Dalton G. CB1 Cannabinoid Receptors and their Associated Proteins. *Curr Med Chem*. 2010;17(14):1382-1393. doi:10.2174/092986710790980023

16. Galiegue S, Mary S, Marchand J, et al. Expression of Central and Peripheral Cannabinoid Receptors in Human Immune Tissues and Leukocyte Subpopulations. *Eur J Biochem*. 1995;232(1):54-61. doi:10.1111/j.1432-1033.1995.tb20780.x

17. Pacher P, Mechoulam R. Is lipid signaling through cannabinoid 2 receptors part of a protective system? *Prog Lipid Res*. 2011;50(2):193-211. doi:10.1016/j.plipres.2011.01.001

18. Hanuš L, Breuer A, Tchilibon S, et al. HU-308: A specific agonist for CB 2 , a peripheral cannabinoid receptor. *Proc Natl Acad Sci*. 1999;96(25):14228-14233. doi:10.1073/pnas.96.25.14228

19. Guindon J, Hohmann AG. Cannabinoid CB 2 receptors: a therapeutic target for the treatment of inflammatory and neuropathic pain. *Br J Pharmacol*. 2008;153(2):319-334. doi:10.1038/sj.bjp.0707531

20. Hussain MT, Greaves DR, Iqbal AJ. The Impact of Cannabinoid Receptor 2 Deficiency on Neutrophil Recruitment and Inflammation. *DNA Cell Biol*. 2019;38(10):1025-1029. doi:10.1089/dna.2019.5024

21. Rizzo MD, Henriquez JE, Blevins LK, Bach A, Crawford RB, Kaminski NE. Targeting Cannabinoid Receptor 2 on Peripheral Leukocytes to Attenuate Inflammatory Mechanisms Implicated in HIV-Associated Neurocognitive Disorder. *J Neuroimmune Pharmacol*. 2020;15(4):780-793. doi:10.1007/s11481-020-09918-7

22. Liu Q-R, Aseer KR, Yao Q, et al. Anti-Inflammatory and Pro-Autophagy Effects of the Cannabinoid Receptor CB2R: Possibility of Modulation in Type 1 Diabetes. *Front Pharmacol*. 2021;12:809965. doi:10.3389/fphar.2021.809965

23. Brennecke B, Gazzi T, Atz K, et al. Cannabinoid receptor type 2 ligands: an analysis of granted patents since 2010. *Pharm Pat Anal*. 2021;10(3):111-163. doi:10.4155/ppa-2021-0002

24. Whiting ZM, Yin J, de la Harpe SM, Vernall AJ, Grimsey NL. Developing the Cannabinoid Receptor 2 (CB2) pharmacopoeia: past, present, and future. *Trends Pharmacol Sci*. 2022;43(9):754-771. doi:10.1016/j.tips.2022.06.010

25. Soethoudt M, Grether U, Fingerle J, et al. Cannabinoid CB2 receptor ligand profiling reveals biased signalling and off-target activity. *Nat Commun*. 2017;8(1):13958. doi:10.1038/ncomms13958

26. Han S, Thoresen L, Jung J-K, et al. Discovery of APD371: Identification of a Highly Potent and Selective CB 2 Agonist for the Treatment of Chronic Pain. *ACS Med Chem Lett*. 2017;8(12):1309-1313. doi:10.1021/acsmedchemlett.7b00396

27. Yacyshyn BR, Hanauer S, Klassen P, et al. Safety, Pharmacokinetics, and Efficacy of Olorinab, a Peripherally Acting, Highly Selective, Full Agonist of the Cannabinoid Receptor 2, in a Phase 2a Study of Patients With Chronic Abdominal Pain Associated With Crohn's Disease. *Crohn's Colitis 360*. 2021;3(1). doi:10.1093/crocol/otaa089

28. van der Stelt M, Cals J, Broeders-Josten S, et al. Discovery and Optimization of 1-(4-(Pyridin-2-yl)benzyl)imidazolidine-2,4-dione Derivatives As a Novel Class of Selective Cannabinoid CB2 Receptor Agonists. *J Med Chem*. 2011;54(20):7350-7362. doi:10.1021/jm200916p

29. Mukhopadhyay P, Baggelaar M, Erdelyi K, et al. The novel, orally available and peripherally restricted selective cannabinoid CB 2 receptor agonist LEI-101 prevents cisplatin-induced nephrotoxicity. *Br J Pharmacol*. 2016;173(3):446-458. doi:10.1111/bph.13338

30. Soethoudt M, Hoorens MWH, Doelman W, Martella A, van der Stelt M, Heitman LH. Structure-kinetic relationship studies of cannabinoid CB 2 receptor agonists reveal substituent-specific lipophilic effects on residence time. *Biochem Pharmacol*. 2018;152:129-142. doi:10.1016/j.bcp.2018.03.018

31. Hua T, Vemuri K, Pu M, et al. Crystal Structure of the Human Cannabinoid Receptor CB1. *Cell*. 2016;167(3):750-762.e14. doi:10.1016/j.cell.2016.10.004

32. Shao Z, Yin J, Chapman K, et al. High-resolution crystal structure of the human CB1 cannabinoid

receptor. *Nature*. 2016;540(7634):602-606. doi:10.1038/nature20613

33. Li X, Hua T, Vemuri K, et al. Crystal Structure of the Human Cannabinoid Receptor CB2. *Cell*. 2019;176(3):459-467.e13. doi:10.1016/j.cell.2018.12.011

34. Hua T, Li X, Wu L, et al. Activation and Signaling Mechanism Revealed by Cannabinoid Receptor-Gi Complex Structures. *Cell*. 2020;180(4):655-665.e18. doi:10.1016/j.cell.2020.01.008

35. Xing C, Zhuang Y, Xu T-H, et al. Cryo-EM Structure of the Human Cannabinoid Receptor CB2-Gi Signaling Complex. *Cell*. 2020;180(4):645-654.e13. doi:10.1016/j.cell.2020.01.007

36. Hua T, Vemuri K, Nikas SP, et al. Crystal structures of agonist-bound human cannabinoid receptor CB1. *Nature*. 2017;547(7664):468-471. doi:10.1038/nature23272

37. Shao Z, Yan W, Chapman K, et al. Structure of an allosteric modulator bound to the CB1 cannabinoid receptor. *Nat Chem Biol*. 2019;15(12):1199-1205. doi:10.1038/s41589-019-0387-2

38. Yang X, Wang X, Xu Z, et al. Molecular mechanism of allosteric modulation for the cannabinoid receptor CB1. *Nat Chem Biol*. 2022;18(8):831-840. doi:10.1038/s41589-022-01038-y

39. McAllister SD, Hurst DP, Barnett-Norris J, Lynch D, Reggio PH, Abood ME. Structural Mimicry in Class A G Protein-coupled Receptor Rotamer Toggle Switches. *J Biol Chem*. 2004;279(46):48024-48037. doi:10.1074/jbc.M406648200

40. Krishna Kumar K, Shalev-Benami M, Robertson MJ, et al. Structure of a Signaling Cannabinoid Receptor 1-G Protein Complex. *Cell*. 2019;176(3):448-458.e12. doi:10.1016/j.cell.2018.11.040

41. Díaz Ó, Dalton JAR, Giraldo J. Revealing the Mechanism of Agonist-Mediated Cannabinoid Receptor 1 (CB1) Activation and Phospholipid-Mediated Allosteric Modulation. *J Med Chem*. 2019;62(11):5638-5654. doi:10.1021/acs.jmedchem.9b00612

42. Bow EW, Rimoldi JM. The Structure–Function Relationships of Classical Cannabinoids: CB1/CB2 Modulation. *Perspect Medicin Chem*. 2016;8:PMC.S32171. doi:10.4137/PMC.S32171

43. Kapur A, Hurst DP, Fleischer D, et al. Mutation Studies of Ser7.39 and Ser2.60 in the Human CB 1 Cannabinoid Receptor: Evidence for a Serine-Induced Bend in CB 1 Transmembrane Helix 7. *Mol Pharmacol*. 2007;71(6):1512-1524. doi:10.1124/mol.107.034645

44. Wang X, Jespers W, Prieto-Díaz R, et al. Identification of V6.51L as a selectivity hotspot in stereoselective A2B adenosine receptor antagonist recognition. *Sci Rep*. 2021;11(1):14171. doi:10.1038/s41598-021-93419-x

45. Xu W, Li J, Chen C, et al. Comparison of the Amino Acid Residues in the Sixth Transmembrane Domains Accessible in the Binding-Site Crevices of μ, δ, and κ Opioid Receptors. *Biochemistry*. 2001;40(27):8018-8029. doi:10.1021/bi002490d

46. Javitch JA, Ballesteros JA, Weinstein H, Chen J. A Cluster of Aromatic Residues in the Sixth Membrane-Spanning Segment of the Dopamine D2 Receptor Is Accessible in the Binding-Site Crevice. *Biochemistry*. 1998;37(4):998-1006. doi:10.1021/bi972241y

47. Lin X, Li M, Wang N, et al. Structural basis of ligand recognition and self-activation of orphan GPR52. *Nature*. 2020;579(7797):152-157. doi:10.1038/s41586-020-2019-0

48. Hanson MA, Roth CB, Jo E, et al. Crystal Structure of a Lipid G Protein–Coupled Receptor. *Science (80-)*. 2012;335(6070):851-855. doi:10.1126/science.1215904

49. Jakowiecki J, Filipek S. Hydrophobic Ligand Entry and Exit Pathways of the CB1 Cannabinoid Receptor. *J Chem Inf Model*. 2016;56(12):2457-2466. doi:10.1021/acs.jcim.6b00499

50. Stanley N, Pardo L, Fabritiis G De. The pathway of ligand entry from the membrane bilayer to a lipid G protein-coupled receptor. *Sci Rep*. 2016;6(1):22639. doi:10.1038/srep22639

51. Szlenk CT, GC JB, Natesan S. Does the Lipid Bilayer Orchestrate Access and Binding of Ligands to Transmembrane Orthosteric/Allosteric Sites of G Protein-Coupled Receptors? *Mol Pharmacol*. 2019;96(5):527-541. doi:10.1124/mol.118.115113

52. Bokoch MP, Jo H, Valcourt JR, et al. Entry from the Lipid Bilayer: A Possible Pathway for Inhibition of a Peptide G Protein-Coupled Receptor by a Lipophilic Small Molecule. *Biochemistry*. 2018;57(39):5748-5758. doi:10.1021/acs.biochem.8b00577

53. Sykes DA, Parry C, Reilly J, Wright P, Fairhurst RA, Charlton SJ. Observed Drug-Receptor Association Rates Are Governed by Membrane Affinity: The Importance of Establishing "Micro-Pharmacokinetic/Pharmacodynamic Relationships" at the β 2 -Adrenoceptor. *Mol Pharmacol*. 2014;85(4):608-617. doi:10.1124/mol.113.090209

54. van der Velden WJC, Heitman LH, Rosenkilde MM. Perspective: Implications of Ligand–Receptor Binding Kinetics for Therapeutic Targeting of G Protein-Coupled Receptors. *ACS Pharmacol Transl Sci*. 2020;3(2):179-189. doi:10.1021/acsptsci.0c00012

55. Motulsky HJ, Mahan LC. The kinetics of competitive radioligand binding predicted by the law of mass action. *Mol Pharmacol*. 1984;25(1):1 LP - 9. http://molpharm.aspetjournals.org/content/25/1/1.abstract.

56. Copeland RA, Pompliano DL, Meek TD. Drug–target residence time and its implications for lead optimization. *Nat Rev Drug Discov*. 2006;5(9):730-739. doi:10.1038/nrd2082

57. Yung-Chi C, Prusoff WH. Relationship between the inhibition constant (KI) and the concentration of inhibitor which causes 50 per cent inhibition (I50) of an enzymatic reaction. *Biochem Pharmacol*. 1973;22(23):3099-3108. doi:10.1016/0006-2952(73)90196-2

58. Mastronarde DN. Automated electron microscope tomography using robust prediction of specimen movements. *J Struct Biol*. 2005;152(1):36-51. doi:10.1016/j.jsb.2005.07.007

59. Punjani A, Rubinstein JL, Fleet DJ, Brubaker MA. cryoSPARC: algorithms for rapid unsupervised cryo-EM structure determination. *Nat Methods*. 2017;14(3):290-296. doi:10.1038/nmeth.4169

60. Heymann JB. Single particle reconstruction and validation using Bsoft for the map challenge. *J Struct Biol*. 2018;204(1):90-95. doi:10.1016/j.jsb.2018.07.003

61. Pettersen EF, Goddard TD, Huang CC, et al. UCSF Chimera?A visualization system for exploratory research and analysis. *J Comput Chem*. 2004;25(13):1605-1612. doi:10.1002/jcc.20084

62. Emsley P, Lohkamp B, Scott WG, Cowtan K. Features and development of Coot. *Acta Crystallogr Sect D Biol Crystallogr*. 2010;66(4):486-501. doi:10.1107/S0907444910007493

63. Adams PD, Afonine P V., Bunkóczi G, et al. PHENIX : a comprehensive Python-based system for macromolecular structure solution. *Acta Crystallogr Sect D Biol Crystallogr*. 2010;66(2):213-221. doi:10.1107/S0907444909052925

64. Chen VB, Arendall WB, Headd JJ, et al. MolProbity : all-atom structure validation for macromolecular crystallography. *Acta Crystallogr Sect D Biol Crystallogr*. 2010;66(1):12-21. doi:10.1107/S0907444909042073

65. Chen C, Okayama H. High-efficiency transformation of mammalian cells by plasmid DNA. *Mol Cell Biol*. 1987;7(8):2745-2752. doi:10.1128/mcb.7.8.2745-2752.1987

Acknowledgements

This work was supported by the National Science Fund for Distinguished Young Scholars 32022038 (Tian Hua, T.H.), the National Natural Science Foundation of China grant 91953202 (Z.-J.L.), the CAS Strategic Priority Research Program XDB37030104 (Zhi-Jie Liu[a,b], Z.-J.L.), the National Natural Science Foundation of China grant 31870744 (T.H.), the National Key Research and Development Program of China grant 2018YFA0507000 (T.H.), the Shanghai Rising-Star Program 20QA1406500 (T.H.); the Dutch Research Council (NWO, Vidi #16573) (Laura H. Heitman[c], L.H.H) and (NWO, Navistroke #15851) (Mario van der Stelt[d], M.v.d.S.). and Intramural Research Program of National Institutes of Health/NIAAA (Pal Pacher, P.P.).

Author contributions: Conceptualization, T.H., Z.J.L., J.B. (Jara Bouma[c]), L.V.d.P. (Laura de Paus[d]), A.P.A.J. (Antonius P.A. Janssen[d]), M.v.d.S., L.H.H and P.P.; Conducting Experiments, X.T.L. (Xiaoting Li[a]), H.C. (Hao Chang[a,b]), J.B., L.V.d.P., C.v.d.H (Cas van der Horst[c]), S.S.K (Sanjay Sunil Kumar[c]), L.J.W. (Lijie Wu[a,b]), Y.N.Y. (Yanan Yu[a,b]), R.J.B.H.N.v.d.B (Richard J. B. H. N. van den Berg[d]), A.P.A.J., M.M. (Mohammed Mustafa[f]), P.M. (Partha Mukhopadhyay[e]) , J.P. (Janos Paloczi[e]); Writing-Original Draft, X.T.L., H.C., J.B., L.V.d.P., A.P.A.J., and P.P.; Writing Review & Editing, M.v.d.S., L.H.H., A.L. (Aron Lichtman[f]), P.P. T.H., and Z.J.L.; Visualization, X.T.L., H.C., J.B., A.P.A.J., P.M., L.J.W.; Supervision, M.v.d.S., L.H.H, P.P., T.H., and Z.J.L

[a]iHuman Institute, ShanghaiTech University, Shanghai 201210, China. [b]School of Life Science and Technology, ShanghaiTech University, Shanghai, China. [c]Division of Drug Discovery and Safety, Leiden Academic Center for Drug Research, Leiden University, Oncode Institute, Leiden, the Netherlands. [d]Department of Molecular Physiology, Leiden Institute of Chemistry, Leiden University, Oncode Institute, Leiden, the Netherlands. [e]Laboratory of Cardiovascular Physiology and Tissue Injury, National Institute of Health/National Institute on Alcohol Abuse and Alcoholism, Rockville, MD, USA. [f]Department of Pharmacology and Toxicology, Virginia Commonwealth University, Richmond, VA, USA.